Sleep as a window into thalamocortical pathology: generative modeling implicates NMDA receptor hypofunction in 22q11.2 deletion syndrome

Lioba C S Berndt [1,2,5] Rose Diebel [1] Nicholas A Donnelly [2,4] Jeremy Hall [3] Marianne B M van den Bree [3] Rick A Adams [5,6] Alexander D Shaw [1] Matt W Jones [2]

1 Department of Psychology, Faculty of Health & Life Sciences, University of Exeter, UK. **2** School of Physiology, Pharmacology and Neuroscience, University of Bristol, UK. **3** Neuroscience and Mental Health Innovation Institute and Centre for Neuropsychiatric Genetics and Genomics, Cardiff University, Cardiff, UK. **4** Avon and Wiltshire Mental Health Partnership NHS Trust, Bristol, UK. **5** Hawkes Institute, University College London, UK. **6** Institute of Cognitive Neuroscience, University College London, UK.

Abstract

Background: 22q11.2 deletion syndrome (22q11.2DS) is a strong genetic risk factor for neuropsychiatric conditions, including schizophrenia, autism, ADHD, and intellectual disability. Sleep disturbances and altered sleep EEG in 22q11.2DS suggest underlying thalamocortical dysfunction. However, EEG alone lacks mechanistic resolution, limiting insight into causal mechanisms and treatment targets. Computational modelling can bridge this gap by inferring synaptic dynamics from EEG data.

Methods: We applied conductance-based Dynamic Causal Modelling to sleep–wake EEG from children with 22q11.2DS (n = 28, M_{age} = 14.6, SD = 3.4) and their neurotypical siblings (n = 17, M_{age} = 13.7, SD = 3.4). We estimated synaptic parameters reflecting AMPA, NMDA, $GABA_A$ and $GABA_B$ receptor conductances across vigilance states. To identify candidate intervention targets, we performed "*in silico* pharmacology", simulating increases and decreases in receptor 'gain' to assess which adjustments best aligned 22q11.2DS EEG with control patterns. We also examined associations with psychiatric symptoms.

Results: Increasing NMDA receptor (NMDA-R) gain consistently improved alignment between 22q11.2DS and sibling neural spectra, especially during N2 (ES = 0.32) and N3 sleep (ES = 0.45). Key contributors were local NMDA-R-mediated recurrent-connections among superficial pyramidal cells, and NMDA-driven excitation from spiny stellate to superficial pyramidal populations. We also found that stronger thalamo-cortical connectivity during N3 was associated with greater sleep problems (β = 0.34, p_{FDR} = 0.006), while stronger AMPA-mediated excitation of superficial interneurons during wakefulness predicted anxiety symptoms (β = −0.32, p_{FDR} = 0.032).

Conclusion: Modelling across sleep–wake states revealed state-dependent synaptic abnormalities in 22q11.2DS, identifying NMDA-R hypofunction as a critical mechanism across sleep stages. These findings highlight the potential of *virtual pharmacology* for predicting receptor-level targets in neurodevelopmental disorders.

This research was funded in whole, or in part, by the Wellcome Trust (226709/Z/22/Z). *For the purpose of Open Access, the author has applied a Creative Commons Attribution (CC BY) public copyright licence to any Author Accepted Manuscript version arising from this submission.*

1 Introduction

22q11.2 deletion syndrome (22q11.2DS) is a recurrent microdeletion syndrome with an estimated prevalence of 1:3000 live births. It confers substantial vulnerability to intellectual disability, autism spectrum disorder (ASD), attention-deficit hyperactivity disorder (ADHD), and epilepsy (Cunningham et al. 2018; Eaton et al. 2019; Niarchou et al. 2014). Notably, 22q11.2DS represents the strongest known genetic risk factor for schizophrenia, with up to 25% of adults getting diagnosed with schizophrenia and 40% developing psychotic conditions more broadly (Karayiorgou et al. 1995; Schneider et al. 2014; Monks et al. 2014). Children and young people with this deletion afford a unique opportunity to examine psychosis risk before onset, prior to the confounding effects of disease progression and antipsychotic medication on phenotypic manifestations and their comorbidities.

Recent research has highlighted disrupted sleep physiology as a key factor in the psychiatric risk associated with 22q11.2DS (O'Hora, Schleifer, and Bearden 2023). Sleep disturbances, including insomnia and sleep fragmentation, are prevalent in 22q11.2DS and co-occur with distinct neural signatures during sleep. For example, altered spindle-slow-wave coupling correlates with the severity of psychopathology (Donnelly et al. 2022). These neurophysiological signatures may reflect cross-diagnostic patterns observed in schizophrenia, ASD, and ADHD (Chouinard et al. 2004; Cohrs 2008; Bartsch et al. 2019; Lehoux, Carrier, and Godbout 2019; Biancardi et al. 2021; Castelnovo et al. 2025), disorders that may share some neurobiological similarities with 22q11.2DS. Such parallels suggest shared mechanisms in sleep-related circuit dysfunction that may transcend current diagnostic boundaries.

To systematically investigate these mechanisms, we established the Sleep Detectives initiative, a multidisciplinary program examining sleep (behaviour and neurophysiology) and cognition in 22q11.2DS and other Copy Number Variants associated with increased risk of psychosis. Our work builds on the findings from a prior sleep EEG study (Donnelly et al. 2022) which demonstrated distinct neural alterations during sleep in individuals with 22q11.2DS compared to sibling controls, including elevated slow-wave and spindle amplitude, as well as stronger spindle-slow-wave coupling. These EEG patterns partially mediated the impact of the deletion on anxiety, ADHD, and ASD symptoms. While these results confirm fundamental differences in neural circuit function, conventional EEG analyses cannot fully capture the underlying synaptic mechanisms, which would have direct implications for both early detection and targeted treatment development, as well as for bridging the gap between genetic risk factors, neurobiological mechanisms, and phenotypic expression in neurodevelopmental disorders.

To address this gap, we turned to neural mass modelling, which provides a mechanistic framework for understanding population-level neural dynamics. These models formalise how synaptic interactions generate emergent oscillatory patterns (Deco et al. 2008). Unlike descriptive (i.e. phenomenological) approaches, neural mass models parameterise physiological properties (e.g., synaptic strengths, time constants) that define a mechanistic landscape of circuit alterations. Dynamic Causal Modelling (DCM) operationalises this framework, inferring hidden synaptic parameters from EEG data by optimising model-generated activity to match observed spectra (Friston, Harrison, and Penny 2003).

To pinpoint synaptic mechanisms underlying sleep disturbances in 22q11.2DS, we employed conductance-based DCM (Friston, Harrison, and Penny 2003). This approach integrates Hodgkin-Huxley-type equations (Hodgkin and Huxley 1952) to simulate thalamocortical dynamics, explicitly parameterising thalamic and cortical populations and synaptic connectivity (Shaw,

Muthukumaraswamy, et al. 2020). We focused on the thalamus given its dual role in sleep regulation—orchestrating spindles and slow waves (Ferrarelli and Tononi 2011; D'Agostino et al. 2018)—and its implication in schizophrenia pathophysiology, where thalamic volume reductions and disrupted connectivity are hallmarks (Buchmann et al. 2014; Ferrarelli, Peterson, et al. 2010), making it particularly relevant for examining early markers of psychosis risk through sleep-related measures in 22q11.2DS.

Building on this generative modelling framework, we asked whether synaptic alterations in 22q11.2DS sleep neurophysiology could be targeted through receptor-specific manipulations. We used Dynamic Causal Modelling to simulate in silico "virtual pharmacology", systematically perturbing receptor-level parameters to identify adjustments that shift 22q11.2DS neural activity toward patterns observed in neurotypical siblings. This approach offers a mechanistic step toward identifying candidate intervention targets in high-risk neurodevelopment.

2 Methods

This study extends the findings of Donnelly et al. 2022 by applying DCM to a subset of the Cardiff University ECHO study dataset, comprising children with 22q11.2 deletion syndrome (*n=28*, age: *M=14.6, SD=3.4*) and sibling controls (*n=17*, age: *M=13.7, SD=3.4*), who took part in a study on sleep involving overnight ambulatory EEG collection (Moulding et al. 2020; Donnelly et al. 2022). While the original study identified distinct sleep patterns (figure 1, section 7.2 in the supplementary materials) and their psychiatric correlates such as anxiety, we now leverage these findings to explore the underlying thalamocortical dynamics through DCM. A detailed description of the original study procedures can be found in section 7.1 of the supplementary materials.

2.1 Computational Modeling

We employed a series of fifteen nested thalamocortical models with increasing complexity to characterise spectral activity in sleep EEG data at sensor Cz. These models systematically varied in their parameterisation of synaptic connections to identify the minimal architecture necessary for capturing the observed dynamics. We fitted the model individually for each participant (both 22q11.2DS and control siblings) to capture person-specific dynamics. This approach allowed us to make group-level inferences while accounting for individual variability.

The 15 models were constructed by systematically including or excluding connections mediated by four key synaptic receptor types (AMPA, NMDA, GABA-A, GABA-B) between eight key neuronal populations: pyramidal cells and interneurons in the superficial layers, spiny stellate cells, pyramidal cells and deep interneurons in deep layers, thalamic projection neurons, thalamic relay, and reticular nucleus. We identified the optimal model using Bayesian Information Criterion and complementary model comparison metrics that balance model fit against complexity.

To ensure interpretability of the estimated parameters, we additionally performed parameter recovery analyses, which confirmed that key synaptic parameters could be robustly estimated from the observed data. Full details of the modelling framework, model selection criteria, and parameter recovery analyses are provided in section 7.3.2 of the supplementary materials.

2.2 Identification of Computational Parameters in 22q11.2DS

Group differences in computational model parameters of the winning model between 22q11.2DS and siblings were identified using Parametric Empirical Bayes (PEB) (Friston, Litvak, et al. 2016; Zeidman et al. 2019), a hierarchical Bayesian implementation of general linear models that accounts for parameter uncertainty and covariance in group-level inferences. In the supplementary materials 7.4, we detail why PEB provides more robust group-level inferences compared to frequentist statistical methods (e.g., t-tests) and, thus, is the method of choice here.

2.3 Mechanism Identification Through Receptor-Wide Perturbations

Having identified group-level differences in synaptic parameters, we next simulated receptor-specific synaptic perturbations to test whether biologically plausible changes could shift 22q11.2DS sleep neurophysiology toward patterns observed in neurotypical siblings. This *in silico "virtual pharmacology"* analysis focused on modulating the gain of each receptor system, mirroring the systemic action of pharmacological interventions that typically target specific receptors (but not, for example, specific neuron

types or specific cortical layers).

To this end, we defined four global receptor gain parameters (c.f. hyperparameters), $\Gamma = \{\gamma_{\text{AMPA}}, \gamma_{\text{NMDA}}, \gamma_{\text{GABA-A}}, \gamma_{\text{GABA-B}}\}$. For each receptor k, we applied a uniform scaling factor $\gamma \in [0, 2]$ (in steps of 0.2) to all synaptic connections mediated by that receptor:

$$n_k(s) = \gamma \cdot n_k^0,$$

where n_k^0 denotes the baseline conductance value, and s indexes simulations. All other receptor systems were held at baseline values. For each perturbation, we simulated power spectral densities across participants, computed the group-averaged PSD for the 22q11.2DS group, and quantified alignment with the sibling control PSD using mean squared error (MSE). A model effect size was computed by comparing the MSE of the perturbed model to that of the baseline model. Statistical significance was evaluated using permutation testing with 1,000 permutations (Nichols and Holmes 2002).

To determine whether the effects of receptor-wide perturbations were driven by specific synaptic pathways, we then conducted a complementary parameter-specific analysis. Let $P = \{p_1, p_2, \ldots, p_n\}$ be the set of receptor-mediated synaptic parameters in the model (e.g., the NMDA conductance from spiny stellate to superficial pyramidal cells). For each parameter $p_i \in P$, we applied a multiplicative scaling factor $\alpha \in [0, 2]$ to the baseline value:

$$p_i(s) = \alpha \cdot p_i^0,$$

while keeping all other parameters fixed. This procedure was repeated across participants and simulations. For each perturbation, we again evaluated the group-level PSD and calculated MSE relative to controls to identify the most impactful individual connections.

2.4 Associations Between Thalamocortical Parameters and Psychiatric and Cognitive Measures

In addition, we examined how thalamocortical model parameters (independent variables) predict psychiatric and cognitive symptoms (dependent variables) in the 22q11.2DS group. The dependent variables comprised two categories: (1) psychiatric symptoms, including symptoms of ADHD, anxiety, ASD, sleep disturbances, and psychotic experiences (supplementary materials 7.1.2), and (2) cognitive measures, including the Cambridge Neuropsychological Test Automated Battery (CANTAB) (Robinson et al. 1999) and the Wisconsin Card Sorting Test (WCST) (details in the supplementary section 7.1.3 and 7.1.4). To manage the high dimensionality of the parameter space, we applied LASSO regression (Tibshirani 1996), employing 5-fold cross-validation to determine the optimal penalty parameter (λ). This regularisation method penalises less informative predictors by shrinking their coefficients to zero, effectively isolating the most relevant parameters. For the final models, we selected the appropriate regression approach based on each measure's distribution characteristics (supplementary materials 7.6) and included age and sex as covariates. For outcomes with significant main effects, we further employed interaction models to formally test whether these associations were moderated by group (22q11.2DS vs. siblings). All statistical tests were subjected to FDR correction.

3 Results

3.1 Combined AMPA, NMDA, GABA-A and GABA-B receptor dynamics optimally modelled EEG during wake and sleep states

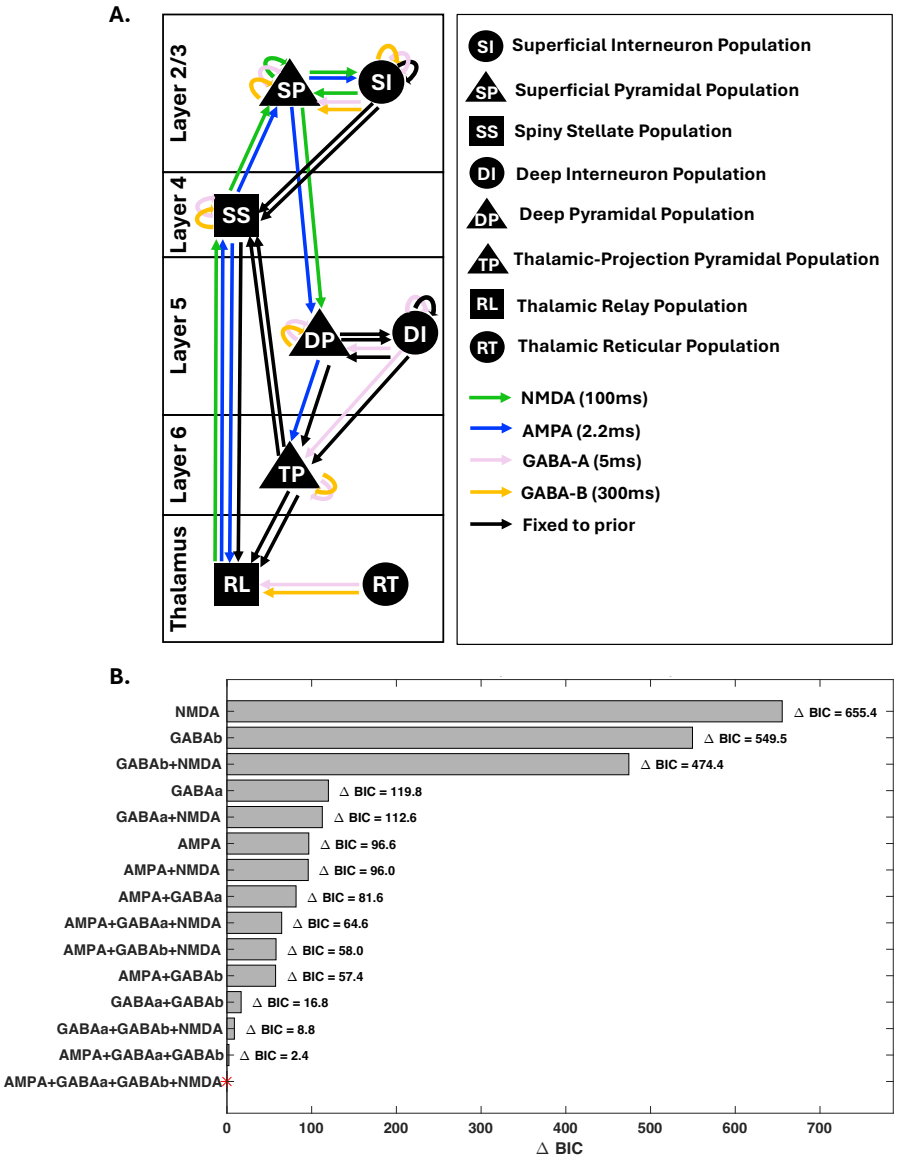

Figure 1: Bayesian Model Comparison. A. Neural circuit architecture of the winning model, illustrating the interactions between different neuronal populations through multiple receptor types. Synaptic connections are mediated by four receptor types with distinct time constants: NMDA (100ms, green), AMPA (2.2ms, blue), GABA-A (5ms, pink), and GABA-B (300ms, yellow). Non-recoverable parameters were fixed to their prior mean (black). **B.** Model comparison results showing ΔBIC values for different receptor combinations in comparison to the winning model. Models are ordered by their evidence, with lower ΔBIC values indicating better model performance.

To identify the optimal combination of glutamatergic and GABAergic receptor types for modelling wake-sleep EEG dynamics, we performed model comparison across models with different combinations of AMPA, NMDA, GABA-A, and GABA-B receptors (figure 1A). The model incorporating all four receptor types (AMPA, NMDA, GABA-A, and GABA-B) emerged as the best explanation of the observed power spectral density when accounting for model complexity, with the lowest BIC value (BIC=24.3). Models including NMDA (ΔBIC = 655.4) or GABA-B (ΔBIC = 549.5) receptors alone showed substantially worse

performance compared to the winning model (figure 1B). Additional model comparison metrics presented in the supplementary materials (section 7.3.2) consistently identified the same winning model, further supporting the robustness of this finding.

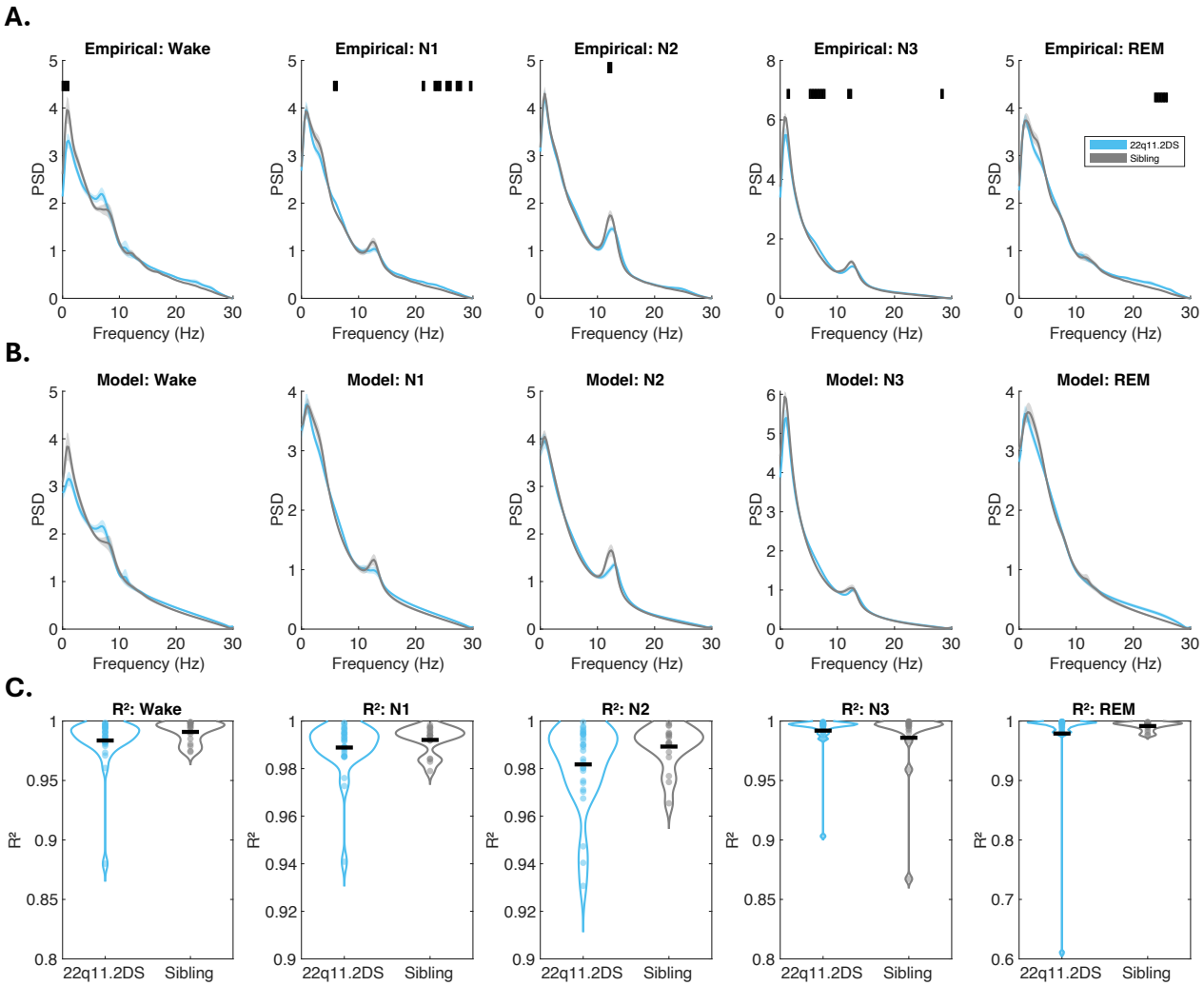

Figure 2: Model Performance Across Sleep Stages. A. Actual empirical spectral densities showing group differences (blue = 22q11.2DS; grey = siblings) at the Cz sensor with significant differences (t-test; $p < 0.05$) marked by black vertical lines. **B.** Model-predicted spectral densities of the winning model. **C.** Variance explained (r^2) by the model for each state, with individual dots representing single participants.

The winning model implements a canonical cortical microcircuit coupled with thalamic populations (figure 1A). The cortical component comprises four layers with distinct neural populations: superficial pyramidal cells (SP) and interneurons (SI) in layer 2/3, spiny stellate cells (SS) in layer 4, deep pyramidal cells (DP) and interneurons (DI) in layer 5 and thalamic projections (TP) neurons in layer 6. These cortical populations interact with thalamic relay (RL) and reticular (RT) nuclei, completing a thalamocortical circuit. Each connection in this architecture is mediated by specific receptor types, with AMPA and NMDA receptors primarily facilitating excitatory transmission, and GABA-A and GABA-B receptors mediating inhibitory signalling, each operating at distinct timescales: fast AMPA (2.2ms), intermediate GABA-A (5ms), slow NMDA (100ms), and very slow GABA-B (300ms). The model successfully captured the empirical spectral differences between 22q11.2DS carriers and siblings across all vigilance states (figure 2A,B). Variance explained (r^2) was consistently high across all states (figure 2C), with mean r^2 values exceeding 0.95 for both groups.

Although the model including all four receptor types provided the best fit to the data, parameter recovery analyses indicated

that several parameters were not reliably identifiable. We therefore fixed these non-recoverable parameters to their prior values (denoted as black arrows in figure 1A) and re-estimated the model for all participants. All results reported are based on this reduced, re-estimated model. Full details on parameter recovery and model re-specification are provided in supplementary section 7.3.2.

3.2 Systematic Increase in Synaptic Alterations from Wake to REM Sleep in 22q11.2 Deletion Syndrome

We used PEB to assess group-level differences in synaptic parameters across vigilance states. The number of parameters showing significant group differences increased from wakefulness to REM sleep, suggesting that synaptic differences between 22q11.2DS carriers and sibling controls became more widespread in later sleep stages. However, the specific connections and receptor types involved varied across stages and did not form a consistent or easily interpretable pattern. Full stage-specific results and visualisations are provided in supplementary section 7.4.1.

3.3 NMDA-R Gain Increase Drives System-Level Alignment between EEG in 22q11.2DS and siblings

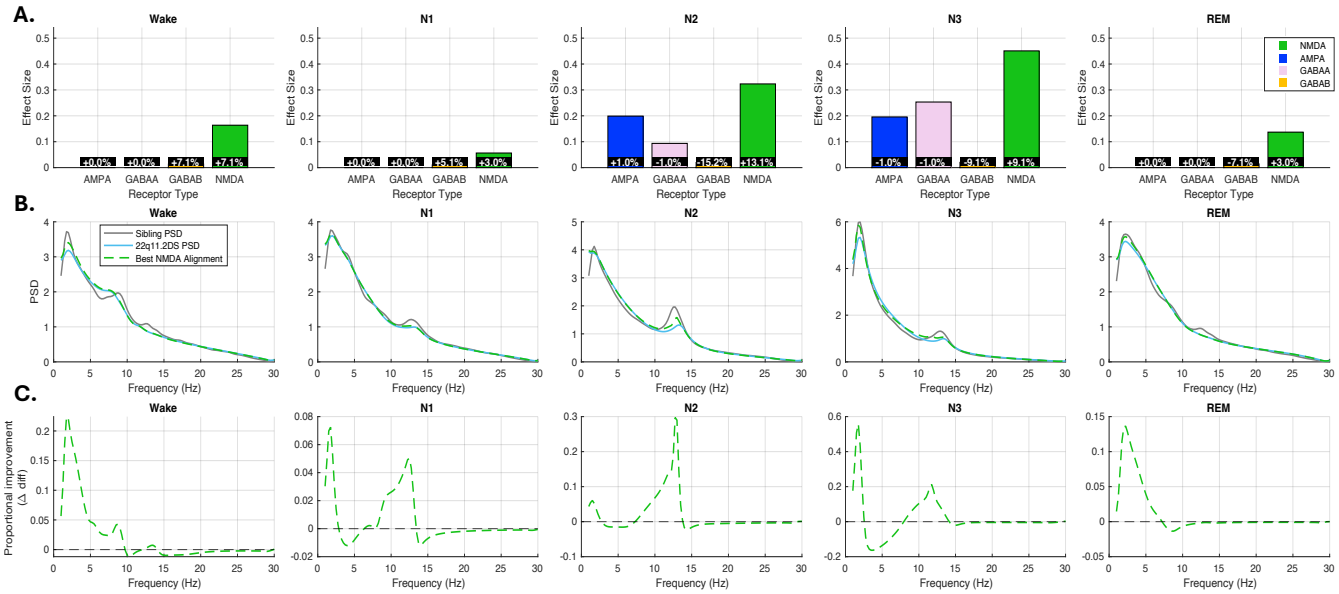

Figure 3: System-wide receptor modulation analysis across vigilance states. Top row: Bar plots show the effect sizes for global gain adjustments in each receptor system. Effect size is defined as the proportional reduction in mean squared error between the group-averaged 22q11.2DS PSD and the sibling control PSD following receptor-specific modulation. Each bar reflects the maximum effect size achieved for that receptor system across the tested gain values. The inset box within each bar indicates the specific per gain adjustment that produced the best alignment. Only NMDA-R gain increases produced consistent and substantial improvements across all vigilance states. **Middle row:** Line plots show PSDs for the sibling control group (grey), the 22q11.2DS group (blue), and the best-fitting NMDA gain simulation (green dashed) for each sleep stage. Simulations reflect the NMDA-R gain parameter setting that yielded the lowest MSE relative to the sibling PSD. **Bottom row:** Frequency-specific proportional improvement in alignment (Δ diff), showing the difference between the baseline and NMDA-R-perturbed mismatch with the sibling PSD. Positive values indicate improved alignment. NMDA-R gain increases primarily enhanced alignment in the delta, theta, and alpha frequency ranges during NREM sleep.

We investigated the potential impact of broad receptor-specific pharmacological interventions by systematically decreasing/increasing the gain of each modelled receptor system (AMPA, $GABA_A$, $GABA_B$, NMDA) across all connections in the model. We evaluated how effectively each manipulation reduced the PSD discrepancy between the 22q11.2DS and sibling control group averages, as measured by the proportional reduction in mean squared error.

Across all vigilance states, increases in NMDA-R gain consistently produced the largest and most reliable improvements in alignment with sibling PSDs. These effects were particularly pronounced during N2 and N3 sleep, yielding effect sizes of 0.32 and 0.45, respectively (figure 3A). Frequency-specific improvements (figure 3B,C) were strongest in the delta and lower theta ranges, with additional gains extending into the spindle frequency range during NREM stages. In lighter sleep stages (N1), REM, and Wake, NMDA-R modulation still yielded significant improvements, albeit with smaller effect sizes (figure 3B,C).

A.

state	dependent variable	model	R^2	independent variable	β	p
wake	anxiety	main	0.25	AMPA (sp→si)	-0.32	**0.032**
				age	-0.20	0.203
				sex	0.12	0.420
				group	0.30	**0.039**
wake	anxiety	interaction	0.25	AMPA (sp→si)	-0.21	0.822
				AMPA (sp→si) × group	-0.23	0.244
				age	-0.23	0.136
				sex	0.09	0.535
				group	0.30	0.151
N3	sleep problems	main	0.33	TC	0.34	**0.026**
				age	-0.17	0.265
				sex	0.14	0.322
				group	0.41	**0.003**
N3	sleep problems	interaction	0.45	TC	0.40	0.854
				TC × group	0.34	**0.006**
				age	-0.17	0.237
				sex	0.12	0.371
				group	0.40	**0.006**

B.

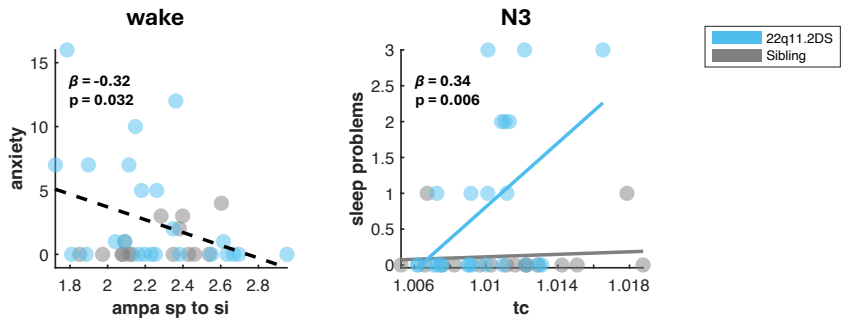

Figure 4: Associations between thalamocortical model parameters and psychiatric symptoms in 22q11.2DS. A. Summary table of significant regression results examining the relationships between thalamocortical model parameters and psychiatric or sleep symptoms. For each sleep state and dependent variable, both main effects and interaction (group × parameter) models are shown. The table reports the model R^2, independent variables, standardised beta coefficients (β), and p-values (p). Significant effects ($p_{FDR} < 0.05$) are highlighted in bold. **B.** Scatter plots illustrating significant associations. Each point represents an individual, with 22q11.2DS participants shown in blue and sibling controls in grey. When there was a significant group × parameter interaction, separate regression lines were shown for each group (blue for 22q11.2DS, grey for siblings). When there was no significant interaction, a single regression line (black, dashed) was shown for all participants.

To determine which specific pathways contributed to these improvements, we then applied targeted parameter perturbations to isolate the effects of individual NMDA-R-mediated synaptic connections. These analyses revealed that the observed alignment benefits were primarily driven by increased NMDA-R conductance on the self-connections of superficial pyramidal cells, and on

the NMDA-R connections from spiny stellate cells to pyramidal cells in the superficial layers (supplementary materials 7.5).

3.4 Associations of AMPA-R-Mediated and Thalamocortical Connectivity with Anxiety and Sleep Problems

Regression analysis showed that during wakefulness, stronger AMPA-R-mediated connectivity from superficial pyramidal cells to interneurons was associated with lower anxiety symptoms across groups (main effect: $\beta = -0.32$, $p_{FDR} = 0.032$), with no significant group interaction (figure 4A,B). In N3 (slow-wave) sleep, increased thalamocortical connectivity was significantly associated with greater sleep problems, and this relationship differed by group (group $\times$ parameter interaction: $\beta = 0.34$, $p_{FDR} = 0.006$, figure 4A,B). No other significant associations were observed. All models included age, sex, and group as covariates.

4 Discussion

In this study, we leveraged computational modelling to infer the synaptic basis of sleep EEG alterations in 22q11.2DS. By systematically perturbing synaptic parameters within a thalamocortical model, we identified alterations that may underlie the observed dynamics. Our central finding was that increasing NMDA receptor gain consistently improved the alignment of 22q11.2DS power spectra with those of neurotypical siblings across all vigilance states, implying NMDA receptor hypofunction as a key driver of altered sleep neurophysiology in 22q11.2DS and highlighting NMDA systems as a potential therapeutic target. In addition to this core result, we found that synaptic alterations became more extensive across sleep stages, and identified associations between specific parameters and psychiatric symptoms, including links between thalamocortical connectivity and sleep problems, and between AMPA-R-related pathways and anxiety.

4.1 Sleep As A Potential Amplifier Of Synaptic Dysfunction

Sleep may amplify synaptic dysfunction in 22q11.2DS. We observed that synaptic alterations, which were relatively subtle during wakefulness, became progressively more pronounced across sleep stages. Sleep here could act like a "stress test" for neural circuits in 22q11.2DS. This process appears to unmask underlying vulnerabilities, potentially being linked to the common observation that sleep disturbances are often associated with more severe psychiatric symptoms in 22q11.2DS (O'Hora, Schleifer, and Bearden 2023) and related neurodevelopmental disorders (Liu et al. 2006; Krakowiak et al. 2008; Hvolby 2015; Singh and Zimmerman 2015; Hertenstein et al. 2019). Alternatively, the more regular and persistent nature of network activity during sleep—characterised by stable oscillatory patterns and reduced variability compared to wakefulness—may make underlying synaptic dysfunctions more apparent (Prerau et al. 2017; Burioka et al. 2005; Steriade 2006).

4.2 Therapeutic Potential of Targeting NMDA Receptor Systems

Our receptor-level perturbation analysis identified NMDA-R gain enhancement as the most effective manipulation for shifting 22q11.2DS network dynamics toward control-like patterns, with consistent effects across all vigilance states. These findings support the hypothesis that glutamatergic dysfunction—specifically, NMDA receptor hypofunction—contributes to altered circuit dynamics in 22q11.2DS.

This aligns with evidence for NMDA receptor hypofunction in mouse models of 22q11.2DS (Didriksen et al. 2017) and with long-standing models of NMDA dysregulation in schizophrenia and related disorders (Coyle 1996; Balu and Coyle 2015; Lee, Choi, and Kim 2015; Dalmau 2016), and reinforces the potential of NMDA-R-targeting compounds—such as positive allosteric modulators or glycine site agonists—for preclinical investigation (Uno and Coyle 2019). That these effects were most pronounced during NREM sleep suggests a role for NMDA-R-dependent processes in shaping slow-wave activity and sleep-related neural dynamics. Because NMDA-R-gain enhancement improved dynamics in wake, NREM and REM alike, it offers a single, stage-invariant mechanism—far simpler to translate pharmacologically than juggling separate, state-specific interventions.

Finally, our findings demonstrate how in silico pharmacology can extend beyond group-level comparisons to test causal hypotheses about synaptic function. By embedding candidate interventions directly within generative models, this approach offers a mechanistically grounded strategy for identifying targets for future translational and preclinical research.

4.3 Altered Thalamocortical and AMPA-Mediated Connectivity are associated with Sleep Disturbances and Anxiety Symptoms

Our findings indicate that sleep problems in 22q11.2DS were most strongly linked to altered thalamocortical connectivity during N3 (deep non-REM) sleep. Specifically, increased thalamocortical connectivity was associated with greater sleep problems, and this relationship was significantly moderated by group, suggesting that the impact of thalamocortical dynamics on sleep quality is heightened in 22q11.2DS. This implicates the core thalamocortical system—critical for generating slow waves and maintaining sleep architecture (Steriade, McCormick, and Sejnowski 1993; Crunelli and Hughes 2010)—in the subjective experience of poor sleep quality in this population. Coordinated interactions between cortical and thalamic networks underlie non-REM sleep oscillations, with cortical downstates triggering thalamic downstates and subsequent spindle generation (Mak-McCully et al. 2017). Disruption of this cortico-thalamo-cortical interplay may therefore contribute to the sleep disturbances commonly reported in 22q11.2DS.

In addition, we found that lower anxiety symptoms were associated with stronger AMPA-R-mediated excitation of superficial interneurons during wakefulness, independent of group. This finding suggests that enhanced feedforward inhibition via AMPA receptors may play a protective role in anxiety regulation. However, this interpretation should be considered in light of pharmacological studies reporting anxiolytic effects of AMPA receptor antagonists (Kapus et al. 2008; Bergink, Van Megen, and Westenberg 2004). The mechanisms underlying this discrepancy require further investigation.

5 Limitations

First, our parameter perturbation approach has inherent constraints. System-wide scaling captures global changes but abstracts away pharmacological specificity, such as receptor subtype selectivity, pharmacokinetics, and off-target effects. Second, the magnitude of simulated changes in PSD resulting from optimal adjustments was consistently small. Although these manipulations minimised the MSE metric, the resulting spectral shifts were subtle, suggesting either limited model sensitivity or that individual parameter changes exert only modest effects. Third, our reliance on group-averaged EEG data masks important sources of inter-individual variability within both 22q11.2DS and control groups. This is particularly significant given the broad age range of our participants (6-20 years), during which the brain undergoes substantial developmental changes. By averaging across this wide age range, we may have obscured important developmental differences in neural dynamics and their modulation, and our findings reflect alignment toward average control patterns rather than personalised trajectories. Fourth, despite using LASSO regularisation to address the high-dimensional nature of our regression analysis, the relatively small sample size compared to the number of predictors remains a limitation.

6 Conclusion

Our findings demonstrate that synaptic circuit alterations in 22q11.2DS are strongly dependent on brain state, with the most pronounced differences emerging during sleep. This state-dependence suggests that static models may miss important aspects of circuit dysfunction and highlights the value of probing neural dynamics across different vigilance states. Motivated by these results, we are now collecting longitudinal EEG and behavioural data to track how synaptic and network changes relate to

clinical symptoms over development. In parallel, mouse models of 22q11.2 deletion will allow tests of the causal impact of specific synaptic perturbations on sleep and network dynamics. By pharmacologically manipulating mouse NMDA receptor systems exactly as predicted by our model, we can directly evaluate which interventions restore network activity toward the control regime before advancing to human trials. If the state-dependent circuit alterations observed in humans are recapitulated in mice, this will provide a platform for targeted pharmacological interventions—such as NMDA receptor modulation—in preclinical models. Ultimately, integrating longitudinal human studies with mechanistic animal work will be essential for translating computational and circuit-level insights into effective, developmentally informed treatments for 22q11.2DS and related neurodevelopmental disorders.

Funding

This work was supported by a Wellcome grant (226709/Z/22/Z).

Financial disclosure

All authors report no biomedical financial interests or potential conflicts of interest.

Data availability statement

This study did not generate any new data. All analyses were conducted on previously published data from the IMAGINE-ID/ECHO study, available as part of the original publication by Donnelly et al. 2022. Source Data files are included with that publication.

Acknowledgments

We gratefully acknowledge Ullrich Bartsch, Hayley A. Moulding, Christopher Eaton, Hugh Marston, Jessica H. Hall, and Michael J. Owen, whose previous work and data collection made this study possible. We thank the Sleep Detectives team for their valuable input during data analysis, modelling, and manuscript preparation. We are especially grateful to the Lived Experience Advisory Group consisting of families with lived experience of 22q11.2DS and their children, plus support charities (Max Appeal and Unique), for their regular input and feedback throughout the project. Finally, we thank all participants and their families for their invaluable contributions to this research.

References

Angold, Adrian et al. (1995). “The child and adolescent psychiatric assessment (CAPA)”. In: *Psychological medicine* 25.4, pp. 739–753.

Avella Gonzalez, Oscar J et al. (2015). “H-channels affect frequency, power and amplitude fluctuations of neuronal network oscillations”. In: *Frontiers in Computational Neuroscience* 9, p. 141.

Balu, Darrick T and Joseph T Coyle (2015). “The NMDA receptor ‘glycine modulatory site’in schizophrenia: D-serine, glycine, and beyond”. In: *Current opinion in pharmacology* 20, pp. 109–115.

Bartsch, Ullrich et al. (2019). “Distributed slow-wave dynamics during sleep predict memory consolidation and its impairment in schizophrenia”. In: *NPJ schizophrenia* 5.1, p. 18.

Bastos, Andre M et al. (2012). “Canonical microcircuits for predictive coding”. In: *Neuron* 76.4, pp. 695–711.

Bergink, Veerle, Harold JGM Van Megen, and Herman GM Westenberg (2004). “Glutamate and anxiety”. In: *European Neuropsychopharmacology* 14.3, pp. 175–183.

Berument, Sibel Kazak et al. (1999). “Autism screening questionnaire: diagnostic validity”. In: *The British Journal of Psychiatry* 175.5, pp. 444–451.

Biancardi, Carlo et al. (2021). “Sleep EEG microstructure in children and adolescents with attention deficit hyperactivity disorder: a systematic review and meta-analysis”. In: *Sleep* 44.7, zsab006.

Bigdely-Shamlo, Nima et al. (2015). “The PREP pipeline: standardized preprocessing for large-scale EEG analysis”. In: *Frontiers in neuroinformatics* 9, p. 16.

Bokil, Hemant et al. (2010). “Chronux: a platform for analyzing neural signals”. In: *Journal of neuroscience methods* 192.1, pp. 146–151.

Bordas, Csilla, Adrienn Kovacs, and Balazs Pal (2015). “The M-current contributes to high threshold membrane potential oscillations in a cell type-specific way in the pedunculopontine nucleus of mice”. In: *Frontiers in cellular neuroscience* 9, p. 121.

Brown, Jon T, Ceri H Davies, and Andrew D Randall (2007). “Synaptic activation of GABAB receptors regulates neuronal network activity and entrainment”. In: *European Journal of Neuroscience* 25.10, pp. 2982–2990.

Buchmann, Andreas et al. (2014). “Reduced mediodorsal thalamic volume and prefrontal cortical spindle activity in schizophrenia”. In: *Neuroimage* 102, pp. 540–547.

Buckelmüller, J et al. (2006). “Trait-like individual differences in the human sleep electroencephalogram”. In: *Neuroscience* 138.1, pp. 351–356.

Burioka, Naoto et al. (2005). “Approximate entropy in the electroencephalogram during wake and sleep”. In: *Clinical EEG and neuroscience* 36.1, pp. 21–24.

Castelnovo, Anna et al. (2025). “Sleep spindle abnormalities as neurophysiological biomarkers of Schizophrenia spectrum disorders: From cellular mechanisms and neural circuits to clinical implications”. In: *Biological Psychiatry*.

Chouinard, Sylvie et al. (2004). “Sleep in untreated patients with schizophrenia: a meta-analysis”. In: *Schizophrenia bulletin* 30.4, pp. 957–967.

Cohrs, Stefan (2008). “Sleep disturbances in patients with schizophrenia: impact and effect of antipsychotics”. In: *CNS drugs* 22, pp. 939–962.

Coyle, Joseph T (1996). “The glutamatergic dysfunction hypothesis for schizophrenia”. In: *Harvard review of psychiatry* 3.5, pp. 241–253.

Crunelli, Vincenzo and Stuart W Hughes (2010). “The slow (< 1 Hz) rhythm of non-REM sleep: a dialogue between three cardinal oscillators”. In: *Nature neuroscience* 13.1, pp. 9–17.

Cunningham, Adam C et al. (2018). “Developmental coordination disorder, psychopathology and IQ in 22q11. 2 deletion syndrome”. In: *The British Journal of Psychiatry* 212.1, pp. 27–33.

D’Agostino, Armando et al. (2018). “Sleep endophenotypes of schizophrenia: slow waves and sleep spindles in unaffected first-degree relatives”. In: *npj Schizophrenia* 4.1, p. 2.

Dalmau, Josep (2016). “NMDA receptor encephalitis and other antibody-mediated disorders of the synapse: The 2016 Cotzias Lecture”. In: *Neurology* 87.23, pp. 2471–2482.

Deco, Gustavo et al. (2008). “The dynamic brain: from spiking neurons to neural masses and cortical fields”. In: *PLoS computational biology* 4.8, e1000092.

Delorme, A and S Makeig (2004). *EEGLAB: an open source toolbox for analysis of single-trial EEG dynamics including independent component analysis. 134, 9–21*.

Delorme, Arnaud, Jason Palmer, et al. (2012). “Independent EEG sources are dipolar”. In: *PloS one* 7.2, e30135.

Didriksen, Michael et al. (2017). “Persistent gating deficit and increased sensitivity to NMDA receptor antagonism after puberty in a new mouse model of the human 22q11. 2 microdeletion syndrome: a study in male mice”. In: *Journal of Psychiatry and Neuroscience* 42.1, pp. 48–58.

Donnelly, Nicholas A et al. (2022). “Sleep EEG in young people with 22q11. 2 deletion syndrome: a cross-sectional study of slow-waves, spindles and correlations with memory and neurodevelopmental symptoms”. In: *Elife* 11, e75482.

Douglas, Rodney J and Kevan AC Martin (2004). “Neuronal circuits of the neocortex”. In: *Annu. Rev. Neurosci.* 27.1, pp. 419–451.

Eaton, Christopher B et al. (2019). “Epilepsy and seizures in young people with 22q11. 2 deletion syndrome: Prevalence and links with other neurodevelopmental disorders”. In: *Epilepsia* 60.5, pp. 818–829.

Ferrarelli, Fabio, Michael J Peterson, et al. (2010). “Thalamic dysfunction in schizophrenia suggested by whole-night deficits in slow and fast spindles”. In: *American Journal of Psychiatry* 167.11, pp. 1339–1348.

Ferrarelli, Fabio and Giulio Tononi (2011). “The thalamic reticular nucleus and schizophrenia”. In: *Schizophrenia bulletin* 37.2, pp. 306–315.

Fleiss, Joseph L (2011). *Design and analysis of clinical experiments*. John Wiley & Sons.

Friston, Karl, Jérémie Mattout, et al. (2007). “Variational free energy and the Laplace approximation”. In: *Neuroimage* 34.1, pp. 220–234.

Friston, Karl J, Lee Harrison, and Will Penny (2003). “Dynamic causal modelling”. In: *Neuroimage* 19.4, pp. 1273–1302.

Friston, Karl J, Vladimir Litvak, et al. (2016). “Bayesian model reduction and empirical Bayes for group (DCM) studies”. In: *Neuroimage* 128, pp. 413–431.

Gandal, MJ et al. (2012). “GABAB-mediated rescue of altered excitatory–inhibitory balance, gamma synchrony and behavioral deficits following constitutive NMDAR-hypofunction”. In: *Translational psychiatry* 2.7, e142–e142.

Gerstner, Wulfram et al. (2014). *Neuronal Dynamics: From Single Neurons to Networks and Models of Cognition*. Cambridge University Press.

Gilbert, Charles D and Torsten N Wiesel (1983). “Functional organization of the visual cortex”. In: *Progress in brain research* 58, pp. 209–218.

Grant, David A and Esta Berg (1948). “A behavioral analysis of degree of reinforcement and ease of shifting to new responses in a Weigl-type card-sorting problem.” In: *Journal of experimental psychology* 38.4, p. 404.

Hertenstein, Elisabeth et al. (2019). “Insomnia as a predictor of mental disorders: a systematic review and meta-analysis”. In: *Sleep medicine reviews* 43, pp. 96–105.

Hodgkin, Alan L and Andrew F Huxley (1952). “A quantitative description of membrane current and its application to conduction and excitation in nerve”. In: *The Journal of physiology* 117.4, p. 500.

Hvolby, Allan (2015). “Associations of sleep disturbance with ADHD: implications for treatment”. In: *ADHD Attention Deficit and Hyperactivity Disorders* 7.1, pp. 1–18.

Jansen, Ben H and Vincent G Rit (1995). “Electroencephalogram and visual evoked potential generation in a mathematical model of coupled cortical columns”. In: *Biological cybernetics* 73.4, pp. 357–366.

Kapus, Gábor L et al. (2008). “Antagonism of AMPA receptors produces anxiolytic-like behavior in rodents: effects of GYKI 52466 and its novel analogues”. In: *Psychopharmacology* 198, pp. 231–241.

Karayiorgou, Mar et al. (1995). “Schizophrenia susceptibility associated with interstitial deletions of chromosome 22q11.” In: *Proceedings of the National Academy of Sciences* 92.17, pp. 7612–7616.

Krakowiak, Paula et al. (2008). “Sleep problems in children with autism spectrum disorders, developmental delays, and typical development: A population-based study”. In: *Journal of sleep research* 17.2, pp. 197–206.

Kullback, Solomon and Richard A Leibler (1951). “On information and sufficiency”. In: *The annals of mathematical statistics* 22.1, pp. 79–86.

Lee, Eun-Jae, Su Yeon Choi, and Eunjoon Kim (2015). “NMDA receptor dysfunction in autism spectrum disorders”. In: *Current opinion in pharmacology* 20, pp. 8–13.

Lehoux, Thomas, Julie Carrier, and Roger Godbout (2019). “NREM sleep EEG slow waves in autistic and typically developing children: Morphological characteristics and scalp distribution”. In: *Journal of Sleep Research* 28.4, e12775.

Liu, Xianchen et al. (2006). “Sleep disturbances and correlates of children with autism spectrum disorders”. In: *Child psychiatry and human development* 37, pp. 179–191.

Mak-McCully, RA et al. (2017). *Coordination of cortical and thalamic activity during non-REM sleep in humans. Nat. Commun. 8.*

Maris, E and R Oostenveld (2007). *Nonparametric statistical testing of EEG-and MEG-data, 164 (1), 177–190.*

Monks, Stephen et al. (2014). “Further evidence for high rates of schizophrenia in 22q11. 2 deletion syndrome”. In: *Schizophrenia research* 153.1-3, pp. 231–236.

Moran, Rosalyn J et al. (2011). “An in vivo assay of synaptic function mediating human cognition”. In: *Current Biology* 21.15, pp. 1320–1325.

Morris, Catherine and Harold Lecar (1981). “Voltage oscillations in the barnacle giant muscle fiber”. In: *Biophysical journal* 35.1, pp. 193–213.

Moulding, HA et al. (2020). “Sleep problems and associations with psychopathology and cognition in young people with 22q11. 2 deletion syndrome (22q11. 2DS)”. In: *Psychological Medicine* 50.7, pp. 1191–1202.

Mullen, Tim R et al. (2015). “Real-time neuroimaging and cognitive monitoring using wearable dry EEG”. In: *IEEE transactions on biomedical engineering* 62.11, pp. 2553–2567.

Niarchou, Maria et al. (2014). “Psychopathology and cognition in children with 22q11. 2 deletion syndrome”. In: *The British Journal of Psychiatry* 204.1, pp. 46–54.

Nichols, Thomas E and Andrew P Holmes (2002). “Nonparametric permutation tests for functional neuroimaging: a primer with examples”. In: *Human brain mapping* 15.1, pp. 1–25.

O’Hora, Kathleen P, Charles H Schleifer, and Carrie E Bearden (2023). “Sleep in 22q11. 2 Deletion Syndrome: Current Findings, Challenges, and Future Directions”. In: *Current Psychiatry Reports* 25.10, pp. 479–491.

Owen, Adrian M et al. (1990). “Planning and spatial working memory following frontal lobe lesions in man”. In: *Neuropsychologia* 28.10, pp. 1021–1034.

Penny, Will D et al. (2010). “Comparing families of dynamic causal models”. In: *PLoS computational biology* 6.3, e1000709.

Peters, H Christian et al. (2005). “Conditional transgenic suppression of M channels in mouse brain reveals functions in neuronal excitability, resonance and behavior”. In: *Nature neuroscience* 8.1, pp. 51–60.

Pinotsis, Dimitris A et al. (2013). “Dynamic causal modelling of lateral interactions in the visual cortex”. In: *Neuroimage* 66, pp. 563–576.

Pion-Tonachini, L, K Kreutz-Delgado, and S Makeig (2019). *ICLabel: An automated electroencephalographic independent component classifier, dataset, and website. NeuroImage, 198, 181e197.*

Prerau, Michael J et al. (2017). “Sleep neurophysiological dynamics through the lens of multitaper spectral analysis”. In: *Physiology* 32.1, pp. 60–92.

Purcell, SM et al. (2017). “Characterizing sleep spindles in 11,630 individuals from the National Sleep Research Resource”. In: *Nature communications* 8.1, p. 15930.

Robinson, SE et al. (1999). *Recent advances in biomagnetism*.

Royston, Patrick (1992). “Approximating the Shapiro-Wilk W-test for non-normality”. In: *Statistics and computing* 2, pp. 117–119.

Sahakian, Barbara J and AM1293547 Owen (1992). “Computerized assessment in neuropsychiatry using CANTAB: discussion paper”. In: *Journal of the Royal Society of medicine* 85.7, p. 399.

Santoro, Bina and Tallie Z Baram (2003). “The multiple personalities of h-channels”. In: *Trends in neurosciences* 26.10, pp. 550–554.

Schneider, Maude et al. (2014). “Psychiatric disorders from childhood to adulthood in 22q11. 2 deletion syndrome: results from the International Consortium on Brain and Behavior in 22q11. 2 Deletion Syndrome”. In: *American Journal of Psychiatry* 171.6, pp. 627–639.

Selyanko, AA and DA Brown (1999). “M-channel gating and simulation”. In: *Biophysical journal* 77.2, pp. 701–713.

Shaw, Alexander D, Rosalyn J Moran, et al. (2017). “Neurophysiologically-informed markers of individual variability and pharmacological manipulation of human cortical gamma”. In: *Neuroimage* 161, pp. 19–31.

Shaw, Alexander D, Suresh D Muthukumaraswamy, et al. (2020). “Generative modelling of the thalamo-cortical circuit mechanisms underlying the neurophysiological effects of ketamine”. In: *NeuroImage* 221, p. 117189.

Singh, Kanwaljit and Andrew W Zimmerman (2015). “Sleep in autism spectrum disorder and attention deficit hyperactivity disorder”. In: *Seminars in pediatric neurology*. Vol. 22. 2. Elsevier, pp. 113–125.

Steriade, Mircea (2006). “Grouping of brain rhythms in corticothalamic systems”. In: *Neuroscience* 137.4, pp. 1087–1106.

Steriade, Mircea, David A McCormick, and Terrence J Sejnowski (1993). “Thalamocortical oscillations in the sleeping and aroused brain”. In: *Science* 262.5134, pp. 679–685.

Tibshirani, Robert (1996). “Regression shrinkage and selection via the lasso”. In: *Journal of the Royal Statistical Society Series B: Statistical Methodology* 58.1, pp. 267–288.

Traub, Roger D. et al. (2005). “Single-Column Thalamocortical Network Model Exhibiting Gamma Oscillations, Sleep Spindles, and Epileptogenic Bursts”. In: *Journal of Neurophysiology* 93.4. PMID: 15525801, pp. 2194–2232. DOI: 10.1152/jn.00983.2004.

Uno, Yota and Joseph T Coyle (2019). “Glutamate hypothesis in schizophrenia”. In: *Psychiatry and clinical neurosciences* 73.5, pp. 204–215.

Usrey, W Martin and Henry J Alitto (2015). “Visual functions of the thalamus”. In: *Annual review of vision science* 1.1, pp. 351–371.

Wechsler, D (1999). “Wechsler abbreviated scale of intelligence”. In: *Psychological Corporation*.

Wen, Haiguang and Zhongming Liu (2016). “Separating fractal and oscillatory components in the power spectrum of neurophysiological signal”. In: *Brain topography* 29, pp. 13–26.

Wilson, Hugh R and Jack D Cowan (1972). “Excitatory and inhibitory interactions in localized populations of model neurons”. In: *Biophysical journal* 12.1, pp. 1–24.

Zeidman, Peter et al. (2019). “A guide to group effective connectivity analysis, part 2: Second level analysis with PEB”. In: *Neuroimage* 200, pp. 12–25.

7 Supplementary Materials

7.1 Original study design

This study was originally reported by Donnelly et al. 2022 and is reproduced here for contextualisation of our modelling approach.

7.1.1 Participants and Recruitment

Participants were recruited through the Experiences of Children with copy number variants (ECHO) study (Moulding et al. 2020). The study included 28 individuals diagnosed with 22q11.2 Deletion Syndrome and 17 unaffected siblings serving as controls, selected based on proximity in age to the affected participant. Given the exploratory nature of this cross-sectional study involving a rare neurodevelopmental condition, the sample size represented the maximum number of participants who consented to undergo EEG recording during the study period. Confirmation of the 22q11.2 deletion status (presence or absence) was obtained from Medical Genetics laboratory reports or through microarray analysis conducted at the MRC Centre for Neuropsychiatric Genetics and Genomics, Cardiff University. Ethical oversight was provided by the NHS Southeast Wales Research Ethics Committee, which approved all study protocols. Informed consent was obtained from primary carers for all participants. Additionally, participants aged 16 years or older who possessed the capacity to consent provided their own assent. Demographic characteristics can be found in supplementary table 1. Within the 22q11.2DS group, prescribed medications included melatonin (n=4), methylphenidate (n=1), and sertraline (n=1). No control participants were taking psychiatric medications. A history of epilepsy or seizure disorder was an exclusion criterion, and no participants reported such conditions. All data collection, including PSG and cognitive tasks, occurred during single visits to the participants' homes. These visits were scheduled for participant convenience, typically on weekends or during school holidays. For sibling pairs, data acquisition was completed within the same visit.

7.1.2 Psychiatric and Cognitive Assessment

Psychopathology symptoms and subjective sleep quality were evaluated using the Child and Adolescent Psychiatric Assessment (CAPA) interview (Angold et al. 1995), administered to either the participant or their primary carer during the home visit. Symptoms related to Autism Spectrum Disorder were screened via the Social Communication Questionnaire (SCQ) (Berument et al. 1999), completed by the primary carer. Cognitive ability, specifically Full-Scale IQ (FSIQ), was assessed using the Wechsler Abbreviated Scale of Intelligence (WASI) (Wechsler 1999).

7.1.3 CANTAB Cognitive Assessment

Cognitive function was assessed using the Cambridge Neuropsychological Test Automated Battery (CANTAB) (Robinson et al. 1999), a computerised set of neuropsychological tests administered on a touchscreen device. The following tests were administered:

Working Memory and Processing Speed. Working memory capacity was assessed using the Spatial Working Memory (SWM) task (Owen et al. 1990), which requires participants to search for tokens hidden in boxes while remembering and avoiding previously searched locations. Processing speed was measured through reaction times across various CANTAB tasks.

Sustained Attention. The Rapid Visual Processing (RVP) (Sahakian and Owen 1992) task was used to assess sustained attention. Participants were required to detect target sequences of digits in a continuous stream of numbers. Performance was quantified using the RVP A' score, a signal detection measure that accounts for both hits and false alarms, providing a measure of sensitivity to the target sequence independent of response tendency.

Planning Ability. Planning ability was assessed using the Stockings of Cambridge (SOC) task (Owen et al. 1990), a computerised version of the Tower of London test. Participants were required to move colored balls in a specified minimum number of moves to match a target arrangement. Three measures were derived:

- SOC Initial Time: Planning time before the first move
- SOC Subsequent Time: Average time for moves after the first move
- SOC Problems Solved: Total number of problems solved in the minimum number of moves

All tests were administered according to standardised CANTAB protocols, with task difficulty increasing progressively based on participant performance. Raw scores were converted to standardised scores based on age-appropriate normative data provided by CANTAB.

7.1.4 Wisconsin Card Sorting Test

The Wisconsin Card Sorting Test (WCST) (Grant and Berg 1948) was administered as an additional measure of executive function, specifically cognitive flexibility and set-shifting abilities. In this computerised version of the test, participants were required to sort cards according to different rules (colour, shape, or number) that changed without warning. The task required participants to identify the current sorting rule through trial-and-error learning and adapt their responses when the rule changed. Performance was measured through several key indices:

- Perseverative Errors: Number of times participants persisted with an incorrect sorting rule despite negative feedback
- Non-perseverative Errors: Number of other types of incorrect responses
- Categories Completed: Number of times participants successfully identified and maintained the correct sorting rule

These measures provided a comprehensive assessment of cognitive flexibility, rule-learning abilities, and the capacity to adapt to changing task demands.

7.1.5 Polysomnography (PSG) Data Acquisition

Overnight PSG recordings were conducted in participants' homes using ambulatory systems to minimise disruption to normal sleep routines. High-density EEG was acquired using a 60-channel Geodesic Net (EGI), connected to a BE Plus LTM amplifier running Galileo software (EBNeuro). Standard PSG signals, including EOG, EMG, ECG, respiratory effort (inductance plethysmography), oxygen saturation (pulse oximetry), and nasal airflow, were recorded using an Embla Titanium amplifier. All signals were digitised at a sampling rate of 512 Hz with an online high-pass filter setting of 0.1 Hz. The EEG was referenced online to the Cz electrode. Participants slept in their own beds and could move freely during the night.

Variable	Group		Type	Statistic	p-value
	22q11.2DS n=28[a]	Sibling n=17[a]		(95% CI)	
Age @ EEG	14.6 (3.4)	13.7 (3.4)	Diff[b]	0.90 [-1.22, 3.01]	0.397
Sex			χ^{2}[c]	0	1
Female	14 (50%)	9 (53%)			
Male	14 (50%)	8 (47%)			
Sleep Problem	1.32 (1.70)	0.24 (0.56)	OR[d]	6.27 [2.12, 18.56]	0.001
FSIQ	76 (13)	105 (27)	Diff[e]	-28.70 [-40.48,-16.92]	<0.001
missing	0	1			
Anxiety Sx	5.0 (7.8)	1.4 (2.8)	OR[d]	3.10 [1.93, 4.99]	<0.001
ADHD Sx	6.0 (6.0)	0.7 (2.1)	OR[d]	9.46 [5.12, 17.48]	<0.001
ASD Sx	11 (6)	1 (2)	OR[d]	7.46 [4.76, 11.70]	<0.001
missing	1	1			
Psychotic Exp			OR[f]	4.05 [0.70, 43.67]	0.096
No PE	18 (64%)	15 (88%)			
PE	10 (36%)	2 (12%)			
N1 (%)	10.4 (4.7)	13.6 (4.3)	Diff[e]	-2.71 [-5.05,-0.36]	0.044
N2 (%)	26.2 (8.2)	27.1 (5.9)	Diff[e]	-1.09 [-5.15, 2.97]	0.620
N3 (%)	30 (7)	25 (6)	Diff[e]	5.47 [1.98, 8.96]	0.009
REM (%)	14.4 (4.6)	18.2 (5.6)	Diff[e]	-4.20 [-7.10,-1.30]	0.012
N1 Lat (min)	23 (18)	21 (9)	Diff[e]	3.49 [-5.54, 12.51]	0.470
REM Lat (min)	143 (69)	140 (49)	Diff[e]	9.37 [-19.31, 38.05]	0.549
Sleep Eff (%)	88 (8)	89 (9)	Diff[e]	-1.85 [-5.83, 2.14]	0.398
TST (min)	456 (122)	485 (79)	Diff[e]	-27.21 [-88.49, 34.08]	0.413
Awakenings	42 (52)	42 (40)	Diff[e]	3.10 [-19.73, 25.93]	0.802

[a] Mean (SD); n (%)
[b] Linear Model; [c] χ^2 Test; [d] GLMM; [e] LMM; [f] Fisher's Test
Sx = Symptoms; Exp = Experiences; Lat = Latency; Eff = Efficiency; TST = Total Sleep Time

Supplementary table 1: Demographic and Psychiatric Characteristics. Table shows demographic information, cognitive abilities (FSIQ), psychiatric symptoms, and sleep architecture metrics, with statistical comparisons between 22q11.2DS (n=28) and sibling control (n=17) groups. Adapted from Donnelly et al. 2022.

7.1.6 Sleep Scoring

Sleep stages were visually scored in 30-second epochs by an experienced technician based on standard AASM criteria, using a montage comprising 6 EEG channels and all auxiliary PSG channels. Epochs containing significant artefact were excluded from subsequent EEG analyses. Standard sleep architecture variables were derived, including total sleep time, sleep efficiency, latencies to N1 and REM sleep, and the percentage of total sleep time spent in N1, N2, N3, and REM sleep stages.

7.1.7 EEG Data Processing

EEG data processing relied on established methodologies implemented in MATLAB (Mathworks, Natick, MA, USA), utilising custom scripts and functions from the EEGLAB toolbox (Delorme and Makeig 2004) where appropriate. Raw EEG data were imported into EEGLAB. The pre-processing pipeline included downsampling to 128 Hz, high-pass filtering at 0.25 Hz, removal of 50 Hz line noise using the PREP plugin (Bigdely-Shamlo et al. 2015), suppression of artefacts using Artifact Subspace Reconstruction (Mullen et al. 2015) via the clean_rawdata plugin, and re-referencing to the common average. Independent Component Analysis (ICA) was performed using the AMICA plugin (Delorme, Palmer, et al. 2012), and components identified as non-brain activity (e.g., ECG, EMG, EOG) by the ICLabel algorithm were removed (Pion-Tonachini, Kreutz-Delgado, and Makeig 2019). An additional automated epoch-level artefact rejection procedure was applied to N2 and N3 sleep epochs combined, using iterative thresholding based on power in specific frequency bands (beta: 16–25 Hz; delta: 1–4 Hz) relative to

surrounding epochs, detection of clipped signals, and outlier detection based on signal Root Mean Square (RMS) and Hjorth parameters (Purcell et al. 2017; Buckelmüller et al. 2006). This channel-wise procedure did not result in significant group differences in the proportion of N2 or N3 data removed. Epochs identified as artefact during the manual sleep scoring process were also marked for exclusion.

Spectrograms representing time-varying power across the night were calculated using the multitaper method (30s window, 10s step, 1 Hz bandwidth) (Bokil et al. 2010). Power spectral density (PSD) for frequencies between 0.25 and 30 Hz was computed for each epoch using Welch's periodogram method (4s Hanning window, 2s step) and expressed in decibels (dB). This calculation was performed on both the original and z-scored EEG signals. To separate oscillatory and aperiodic signal components, the Irregular Resampling Auto-Spectral Analysis (IRASA) method was applied (Wen and Liu 2016). Group differences in PSD at each frequency were statistically assessed using linear mixed models, with cluster-based permutation tests applied to correct for multiple comparisons across frequencies (Maris and Oostenveld 2007).

7.2 EEG spectral power at Cz Electrode across sleep stages for 22q11.DS and their siblings.

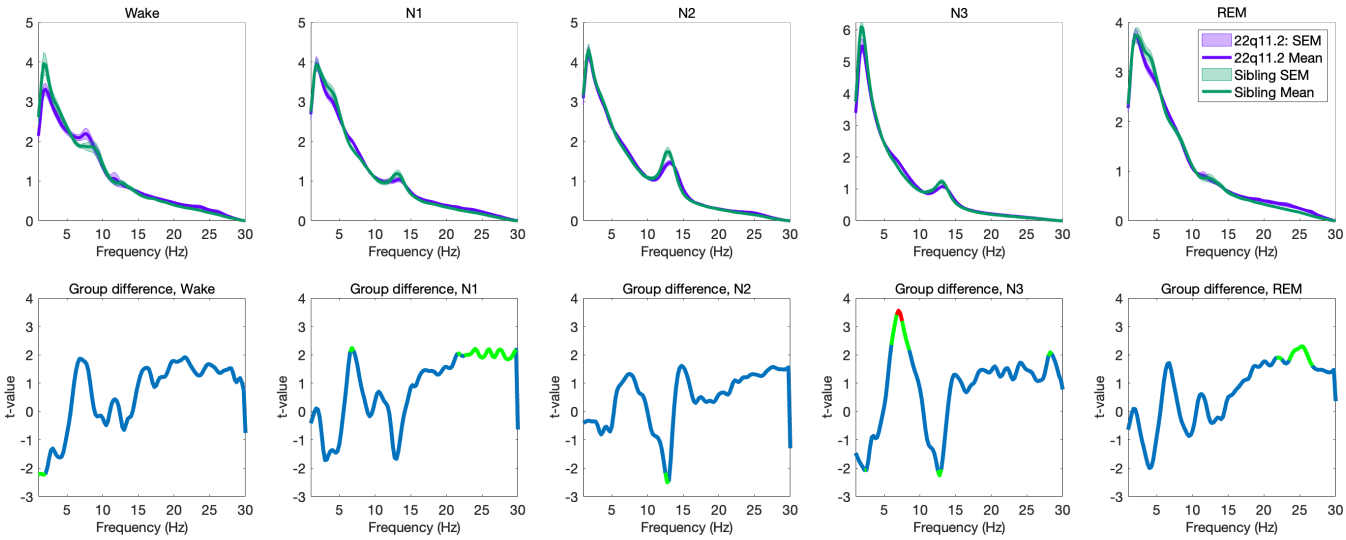

Supplementary figure 1: EEG Spectral Power at Cz Electrode Across Sleep Stages. The Cz electrode showed the most pronounced group differences in power spectral density (PSD), as previously reported by Donnelly et al. 2022. **Top row:** Mean spectral power (±SEM) at the Cz electrode for individuals with 22q11.2 deletion syndrome (purple) and their sibling controls (green) across Wake, N1, N2, N3, and REM sleep stages. The x-axis shows frequency (Hz), and the y-axis shows power (μV^2/Hz, log scale). **Bottom row:** T-values indicating group differences in spectral power across frequencies. Positive t-values (above zero) reflect greater power in the 22q11.2 group, while negative t-values (below zero) indicate reduced power relative to sibling controls.

Donnelly et al. 2022 reported the most pronounced differences in spectral power between 22q11.2DS individuals and their siblings at the Cz electrode. These differences are illustrated in supplementary figure 1 and lay the foundation for our subsequent modelling.

7.3 Thalamo-Cortical-Modelling

We employed Dynamic Causal Modelling (Friston, Harrison, and Penny 2003) to analyse spectral densities in EEG signals. DCM utilises parameterised dynamical systems models, specifically state-space formulations of differential equations—so-

called neural mass models—which describe how variables of interest (e.g., membrane potentials) evolve as a function of connectivity parameters (Friston, Harrison, and Penny 2003). We utilised the thalamo-cortical DCM variant developed by Shaw, Muthukumaraswamy, et al. 2020, which explicitly models interactions between cortical layers and thalamic nuclei.

7.3.1 Modelling procedure

Model Architecture. The thalamo-cortical model incorporates interacting, layer-resolved cortical and thalamic populations, following architectures described by Douglas and Martin 2004, and Gilbert and Wiesel 1983. The model is based on conductance-based equations inspired by the Hodgkin–Huxley and Morris–Lecar formalisms (Morris and Lecar 1981). It includes pyramidal and interneuron populations in cortical layers 2/3 and 5, stellate cells in layer 4, thalamic-projection pyramidal cells in layer 6, and thalamic relay and reticular populations (Traub et al. 2005).

Population dynamics are governed by the following set of coupled differential equations:

$$C\frac{dV}{dt} = \sum_n g_n(V - V_n) + u \tag{1}$$

$$\dot{g}_n = \kappa_n(\varsigma_n - g_n) \tag{2}$$

$$\varsigma = \gamma_{i,j}\,\sigma(\mu_j v - V_R, \Sigma_j) \tag{3}$$

Here, V represents the membrane potential, g_n denotes conductance due to receptor n, and V_n is the corresponding reversal potential. C is the membrane capacitance, and u represents external or internal input currents. κ_n is the decay rate of channel n, $\gamma_{i,j}$ the coupling parameter between populations i and j, and σ is a sigmoid function converting membrane potential into population firing rates.

The model includes AMPA, NMDA, GABA-A, GABA-B, M-type, and H-type conductance channels. M and H channels are specific to layer 6 thalamic-projecting pyramidal cells and thalamic relay populations, facilitating their characteristic bursting behaviour. Building on Moran et al.'s NMDA model (Moran et al. 2011), we incorporate a voltage-dependent magnesium block for NMDA receptors:

$$f_{\mathrm{MG}}(V) = \frac{1}{1 + 0.2\exp(-\alpha_{\mathrm{NMDA}}V)} \tag{4}$$

Reversal potentials and decay rates were derived from established literature to ensure physiological accuracy (Gerstner et al. 2014; Usrey and Alitto 2015; Selyanko and Brown 1999). M-channels influence intrinsic membrane dynamics and the excitation–inhibition balance, while H-channels affect resting membrane potential and network oscillations (Bordas, Kovacs, and Pal 2015; Peters et al. 2005; Santoro and Baram 2003; Avella Gonzalez et al. 2015). GABA-B receptors contribute to macroscale oscillations, particularly in the gamma range (Brown, Davies, and Randall 2007; Gandal et al. 2012).

Generative Model Specification. Following standard spectral DCM approaches, we computed the power spectrum using the Laplace transform. After performing a local linearisation by numerically computing the system's Jacobian about a fixed point, we derived the transfer function from this linearised approximation. The Laplace transform at frequency i, in hertz, is given by:

$$H(s) = C\,(sI - A)^{-1}\,B \tag{5}$$

$$\mathcal{L}\ (\omega_i)\ = C(1\mathbf{i} * 2\pi * \omega_i * I - A)^{-1}B \tag{6}$$

Here, equation (5) represents the "canonical form" Laplace transform, where *H(s)* is the transfer function and *s* is the complex Laplace variable. Equation (6) shows the Laplace transform evaluated at specific frequency *w(i)* in hertz. *A* represents the system Jacobian matrix (*df/dx*), *B* the input Jacobian (*df/du*), and *C* a vector of fixed weights determining each state element's contribution to the output local field potential. This transfer function approach offers computational efficiency compared to numerical integration of model equations. Unlike conventional spectral DCM, we did not explicitly include spectral noise components such as 1/f "aperiodic" components or a discrete cosine basis set for frequency-domain neuronal fluctuations. The model output consists solely of the Laplace transform of the model fitted to data, assuming white noise input.

Model Optimisation and Free Energy. Model parameters were optimised using variational Bayes to maximise the free energy (Friston, Mattout, et al. 2007), which provides a lower bound on the log model evidence. The free energy F is defined as:

$$F = \underbrace{\langle \ln p(y \mid \theta, m) \rangle_q}_{\text{accuracy}} - \underbrace{KL[q(\theta) \parallel p(\theta \mid m)]}_{\text{complexity}} \tag{7}$$

Here, $p(y \mid \theta, m)$ denotes the likelihood of the observed data y given parameters θ under model m, and $q(\theta)$ is the approximate posterior distribution over parameters. The term $KL[q(\theta) \parallel p(\theta \mid m)]$ is the Kullback–Leibler divergence (Kullback and Leibler 1951) between the approximate posterior and the prior distribution $p(\theta \mid m)$.

This framework offers a principled trade-off between model accuracy and complexity (Friston, Harrison, and Penny 2003), mitigating overfitting while ensuring that the model captures essential features of the observed spectra.

Optimisation was performed using an Expectation-Maximisation scheme for each individual, which iteratively updates the posterior distributions of parameters until convergence. This yields both optimal parameter estimates and their associated uncertainties, enabling robust statistical inference about group differences between individuals with 22q11.2DS and their siblings.

Model priors.

Name	**Prior mean**	**Prior variance**
AMPA_ss_to_sp	2	1/8
AMPA_ss_to_rl	2	1/8
AMPA_sp_to_si	2	1/8
AMPA_sp_to_dp	2	1/8
AMPA_dp_to_di	2	1/8
AMPA_dp_to_tp	2	1/8
AMPA_tp_to_ss	2	1/8
AMPA_tp_to_rl	2	1/8
AMPA_rl_to_ss	2	1/8
GABAA_ss_to_ss	8	1/8

GABAA_sp_to_sp	18	1/8
GABAA_si_to_ss	10	1/8
GABAA_si_to_sp	10	1/8
GABAA_si_to_si	10	1/8
GABAA_dp_to_dp	8	1/8
GABAA_di_to_dp	6	1/8
GABAA_di_to_di	14	1/8
GABAA_di_to_tp	6	1/8
GABAA_tp_to_tp	8	1/8
GABAA_rt_to_rl	8	1/8
NMDA_ss_to_sp	2	1/8
NMDA_ss_to_rl	2	1/8
NMDA_sp_to_sp	2	1/8
NMDA_sp_to_si	2	1/8
NMDA_sp_to_dp	2	1/8
NMDA_si_to_sp	2	1/8
NMDA_si_to_si	2	1/8
NMDA_dp_to_di	2	1/8
NMDA_dp_to_tp	2	1/8
NMDA_tp_to_ss	2	1/8
NMDA_tp_to_rl	2	1/8
NMDA_rl_to_ss	2	1/8
GABAB_ss_to_ss	8	1/8
GABAB_sp_to_sp	18	1/8
GABAB_si_to_ss	10	1/8
GABAB_si_to_sp	10	1/8
GABAB_si_to_si	10	1/8
GABAB_dp_to_dp	8	1/8
GABAB_di_to_dp	6	1/8
GABAB_di_to_di	14	1/8
GABAB_di_to_tp	6	1/8
GABAB_tp_to_tp	8	1/8
GABAB_rt_to_rl	8	1/8
Thalamo-Cortical delay	3 ms	1/8
Cortico-Thalamic Delay	8 ms	1/8
scale_NMDA	1	1/8

Electrode Gain	1	1/8

Supplementary table 2: Prior means and variances for thalamo-cortical and cortical-cortical synaptic parameters across different receptor types (AMPA, GABA-A, NMDA, and GABA-B) used during model fitting.

7.3.2 Model Comparison

Model development. The thalamo-cortical model, first introduced by Shaw, Muthukumaraswamy, et al. 2020 and implemented in this study, represents the culmination of decades of neural–mass model work that has progressively incorporated greater anatomical and physiological detail in order to capture the full neural spectrum. In order to provide context and explain why such model complexity is necessary for investigating sleep neurophysiology, we outline the historical development of neural mass models.

The seminal equations of Wilson and Cowan 1972 described interacting excitatory (E) and inhibitory (I) populations and established the mathematical foundations of neural-mass modelling. Although highly abstract, these E–I models demonstrated how macroscopic oscillations can emerge from coupled cortical populations. Jansen and Rit 1995 extended the E–I framework to a cortical column comprising pyramidal cells, excitatory interneurones and inhibitory interneurones. With distinct synaptic time-constants this three-population model reproduced the α-band oscillations that dominate wakeful EEG. Dynamic Causal Modelling embedded these neural equations in a Bayesian inversion framework (Friston, Harrison, and Penny 2003), allowing synaptic parameters to be estimated directly from empirical data. To account for laminar organisation and pharmacological manipulations, the canonical microcircuit (CMC) introduced superficial and deep pyramidal layers together with receptor-specific AMPA, NMDA and $GABA_A$ conductances (Bastos et al. 2012; Pinotsis et al. 2013). This architecture successfully captured faster β/γ activity and permitted quantitative assays of drug actions on glutamatergic and GABAergic signalling (Shaw, Moran, et al. 2017).

Purely cortical models, however, cannot reproduce oscillations that depend on thalamo-cortical loops and slow inhibitory kinetics. To overcome these limitations, Shaw, Muthukumaraswamy, et al. 2020 augmented the CMC with thalamic relay (RL) and reticular (RT) nuclei plus corticothalamic projection neurones, yielding an eight-population circuit (five cortical, three thalamic). Critically, the TCM incorporates slow $GABA_B$ inhibition as well as intrinsic M- and H-type currents, features that are essential for reproducing sleep-stage–specific EEG, including spindles and slow-wave activity. Because our research question concerns synaptic mechanisms of sleep in 22q11.2DS—a condition where both cortical and thalamic circuitry are implicated—the TCM provides the minimum biological detail required. Accordingly, the Bayesian model comparison and parameter-recovery analyses reported below are conducted within this thalamo-cortical model family.

Nested Model Construction. To systematically evaluate the contribution of different synaptic receptor systems in this thalamo-cortical network, we constructed 15 nested models with varying synaptic connectivity patterns (supplementary figure 2). Each model represents a hypothesis about the essential receptor-mediated connections required to generate sleep-stage specific EEG patterns. The models were constructed by systematically including or excluding connections mediated by four key synaptic receptor types (AMPA, NMDA, GABA-A, GABA-B) between eight key regions: Superficial Pyramidal cells (SP), Superficial Interneurons (SI), Spiny Stellate cells (SS), Deep Pyramidal cells (DP), Deep Interneurons (DI), Thalamic Projection neurons

(TP), Thalamic Relay (RL), and Reticular nucleus (RT).

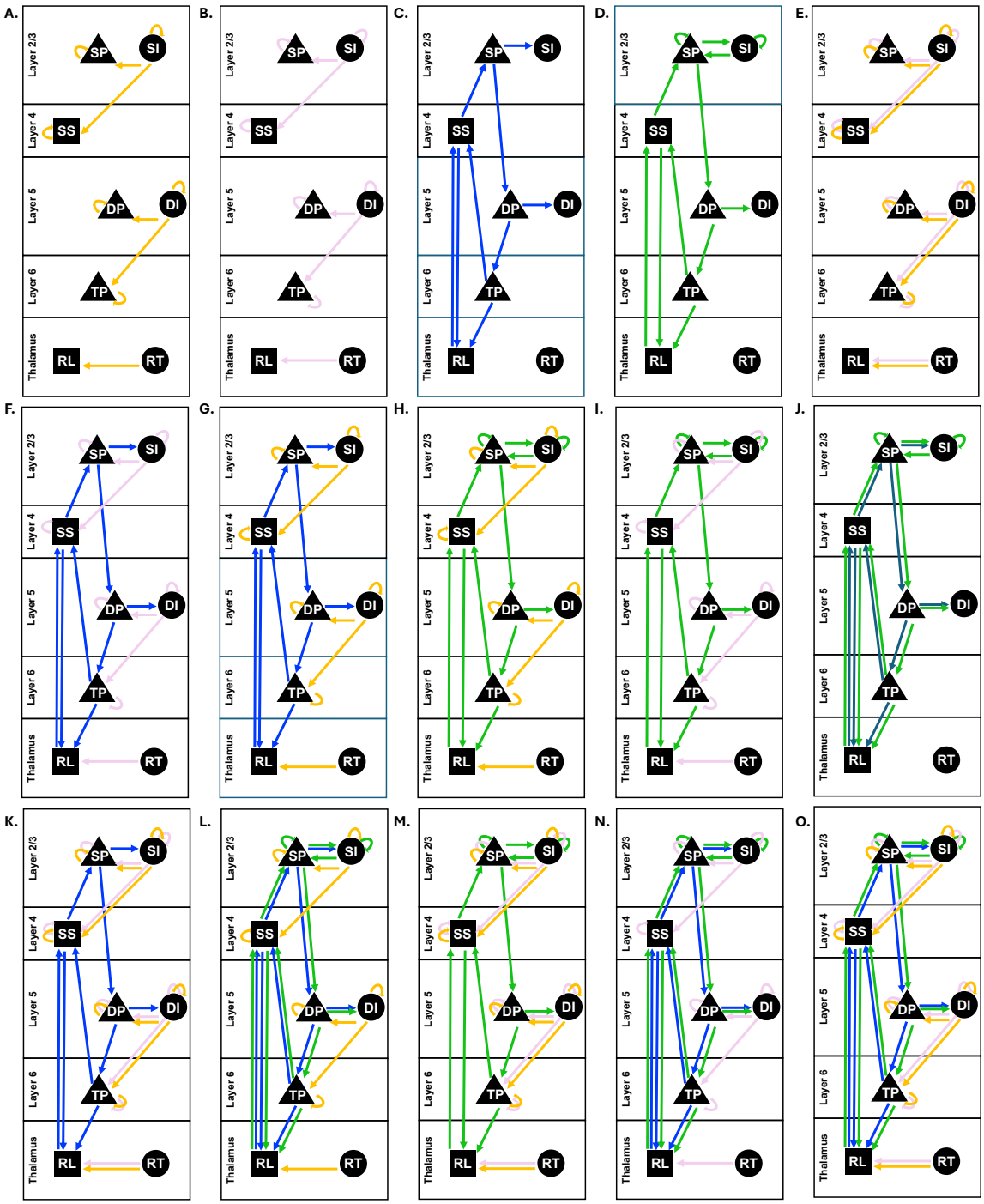

Supplementary figure 2: Nested Models of Receptor-Specific Connectivity. Schematic representation of 15 nested dynamic causal models (A-O) showing different receptor-mediated connectivity patterns in the thalamo-cortical network. Each panel represents a distinct model with specific synaptic connections. Regions are organised in anatomical layers: Layer 2/3, Layer 4, Layer 5, Layer 6, and Thalamus with different neural populations: SP (Superficial Pyramidal), SI (Superficial Interneurons), SS (Spiny Stellate), DP (Deep Pyramidal), DI (Deep Interneurons), TP (Thalamic Projection), RL (Relay), and RT (Reticular nucleus). Arrows indicate directed connections, with colours representing different receptor types: blue: AMPA receptors (fast ionotropic glutamate receptors); pink: GABA-A receptors (fast ionotropic GABA receptors); yellow: GABA-B receptors (slow metabotropic GABA receptors); green: NMDA receptors (slow ionotropic glutamate receptors).

Bayesian Model Comparison of Receptor-Mediated Connections. Having established our 15 nested models of increasing complexity, we next performed a systematic Bayesian model comparison to determine which combination of receptor-mediated connections best explains the observed sleep EEG data.

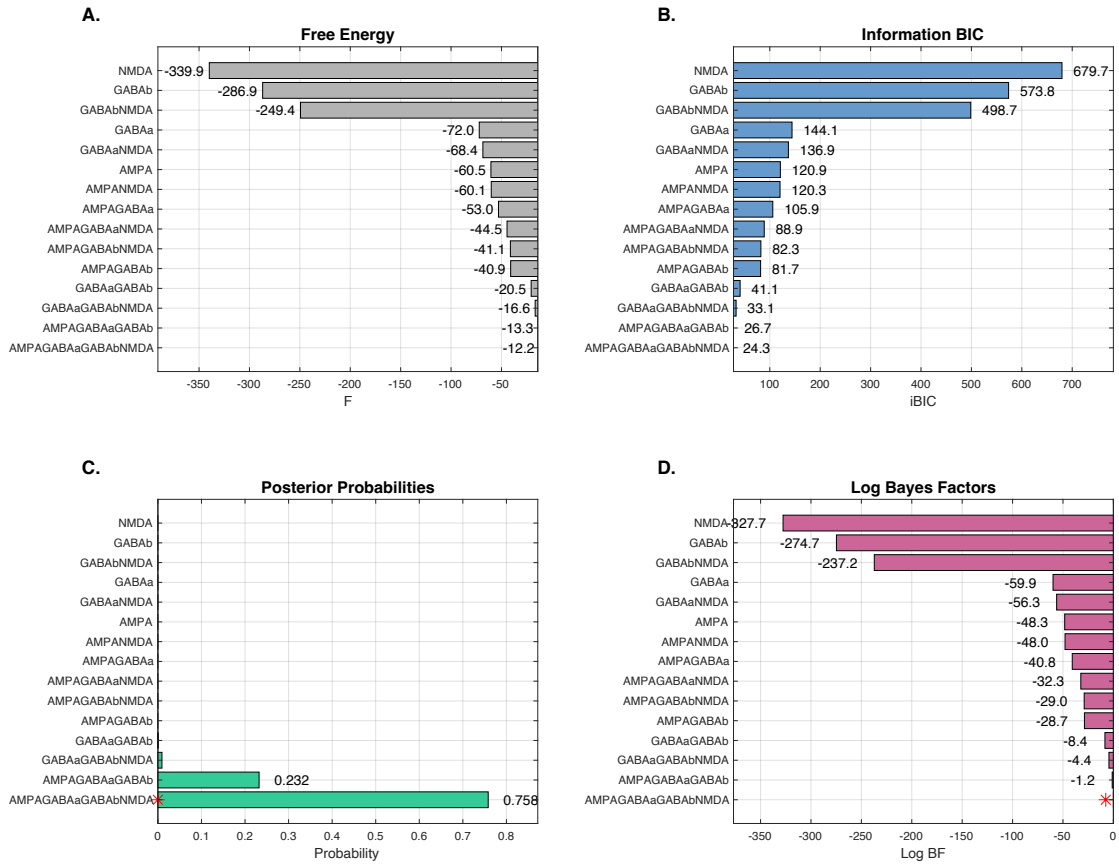

Supplementary figure 3: Bayesian Model Comparison Metrics. Comparison of 15 nested models with different combinations of receptor-mediated connections using four Bayesian model comparison metrics. **(A)** Free energy (F) values for each model, where higher (less negative) values indicate better model evidence. **(B)** Information Bayesian Information Criterion (iBIC) scores, with lower values indicating better model parsimony. The full model achieves the lowest iBIC (24.3), suggesting optimal balance between accuracy and complexity. **(C)** Posterior probabilities showing the relative likelihood of each model given the data, with the full model achieving the highest probability of 0.758. **(D)** Log Bayes Factors comparing each model against the winning model, where more negative values indicate stronger evidence against that model. Model names indicate included receptor types. The progressive improvement in metrics with additional receptor types suggests that each receptor system contributes meaningfully to generating sleep-stage specific EEG patterns.

To quantitatively evaluate these models, we employed four complementary metrics:

1. **Variational Free Energy (F)**: A lower bound on the log model evidence that balances model accuracy with complexity:

$$F = \mathbb{E}_{q(\theta)}[\ln p(y \mid \theta, m)] - KL[q(\theta) \parallel p(\theta \mid m)] \tag{8}$$

where $q(\theta)$ is the approximate posterior, $p(\theta \mid m)$ is the prior, and $p(y \mid \theta, m)$ is the likelihood. Higher (i.e., less negative) free energy values indicate better model evidence by favouring accurate yet parsimonious models.

2. **Bayesian Information Criterion (iBIC)**: A complexity-penalised criterion for model comparison, computed as:

$$\text{iBIC} = -2 \ln p(y \mid \hat{\theta}, m) + k \ln n \tag{9}$$

where $\hat{\theta}$ denotes the maximum a posteriori estimate of the parameters, k is the number of free parameters, and n is the number of observations. Lower iBIC values indicate better model fits.

3. **Posterior Model Probability**: The probability of each model m given the data y, calculated using softmax over the free energies of all candidate models:

$$p(m \mid y) = \frac{\exp(F_m)}{\sum_i \exp(F_i)} \tag{10}$$

where F_m is the free energy of model m. This provides a probabilistic ranking of models.

4. **Log Bayes Factors (lnBF)**: The logarithmic difference in model evidence between each model and the best-performing (winning) model:

$$\ln \text{BF} = F_{\text{winning}} - F_{\text{model}} \tag{11}$$

Our analysis revealed a clear hierarchy in model evidence (supplementary figure 3). The model incorporating all four receptor types (AMPA, GABA-A, GABA-B, NMDA) showed the highest posterior probability (0.758) and highest free energy (-12.2). This model also achieved the lowest iBIC (24.3), indicating it provides the optimal balance between model fit and complexity. The second most probable model (AMPA, GABA-A, GABA-B, probability = 0.232) also performed well, suggesting that a simplified model might be sufficient for some applications. Notably, models with single receptor types showed poor performance, with NMDA-only and GABA-B-only models showing particularly low free energy values (-339.9 and -286.9 respectively) and high iBIC scores (679.7 and 573.8). This indicates that no single receptor type can adequately explain the complex dynamics of sleep-stage transitions. The progressive improvement in model evidence metrics as receptor types are combined suggests that each receptor system plays a distinct and necessary role in generating sleep-stage specific EEG patterns.

7.3.3 Parameter Recovery

To ensure reliable parameter estimation and validate our model's ability to recover true parameter values, we performed parameter recovery analyses. This involved generating synthetic data from known parameter values and then fitting our thalamo-cortical model to these data to assess recovery accuracy.

We simulated EEG spectra using parameter values drawn from physiologically plausible ranges, then fitted the model to these synthetic data using the same optimization procedures as applied to empirical data. Parameter recovery was quantified using Intraclass Correlation Coefficients (ICC) between true and recovered parameter values, providing a measure of estimation reliability across the parameter space.

Parameter	ICC
AMPA	
AMPA_ss_to_sp	0.807
AMPA_ss_to_rl	0.936
AMPA_sp_to_si	0.800
AMPA_sp_to_dp	0.528
AMPA_dp_to_di	Fixed
AMPA_dp_to_tp	0.791
AMPA_tp_to_ss	Fixed
AMPA_tp_to_rl	Fixed
AMPA_rl_to_ss	0.891
GABA-A	
GABA-A_ss_to_ss	0.779
GABA-A_sp_to_sp	0.825
GABA-A_si_to_ss	Fixed
GABA-A_si_to_sp	0.467
GABA-A_si_to_si	0.982
GABA-A_dp_to_dp	0.650
GABA-A_di_to_dp	0.706
GABA-A_di_to_di	0.776
GABA-A_di_to_tp	0.872
GABA-A_tp_to_tp	0.836
GABA-A_rt_to_rl	0.586
NMDA	
NMDA_ss_to_sp	0.731
NMDA_ss_to_rl	Fixed
NMDA_sp_to_sp	0.847
NMDA_sp_to_si	0.613
NMDA_sp_to_dp	0.750
NMDA_si_to_sp	0.636
NMDA_si_to_si	Fixed
NMDA_dp_to_di	Fixed
NMDA_dp_to_tp	Fixed
NMDA_tp_to_ss	Fixed
NMDA_tp_to_rl	Fixed
NMDA_rl_to_ss	0.650
GABA-B	
GABA-B_ss_to_ss	0.940
GABA-B_sp_to_sp	0.903
GABA-B_si_to_ss	Fixed
GABA-B_si_to_sp	0.769
GABA-B_si_to_si	0.890
GABA-B_dp_to_dp	0.896
GABA-B_di_to_dp	Fixed
GABA-B_di_to_di	Fixed
GABA-B_di_to_tp	Fixed
GABA-B_tp_to_tp	0.583
GABA-B_rt_to_rl	0.903
Other	
TC	0.891
CT	0.855
scale_NMDA	0.820

Supplementary table 3: ICC for parameter recovery analysis. Parameters with ICC values < 0.4 were fixed at their prior values. All further analysis were performed on this reduced model.

To maximize the number of interpretable parameters while ensuring estimation reliability, we employed an iterative parameter fixing strategy. In the first iteration, we identified parameters that remained at their prior values across participants, indicating

they were not contributing to model fit, and fixed these at their prior values. We then re-ran parameter recovery to assess how ICC values changed. In the second iteration, we fixed only parameters with ICC values below 0.2, representing the most unreliable estimates, and again re-ran parameter recovery. Finally, in the third iteration, we assessed whether any remaining parameters had ICC values below 0.4 (Fleiss 2011), fixing these. This iterative approach prioritizes retaining as many parameters as possible for biological interpretation while ensuring that only well-constrained parameters contribute to our group-level inferences, reducing the risk of spurious findings while maintaining the model's ability to capture meaningful neurophysiological differences. This procedure resulted in ICC values > 0.4 for all retained parameters (supplementary table 3), with many of these parameters reaching ICC values > 0.70, placing them in the good-excellent range (as suggested by Fleiss 2011).

7.4 Parametric Empirical Bayes Analysis of Group Differences

Following the initial model comparison which established the optimal thalamocortical architecture common to all subjects, we employed Parametric Empirical Bayes (PEB; `spm_dcm_peb`) (Friston, Litvak, et al. 2016; Zeidman et al. 2019) to specifically investigate differences in synaptic parameters within this winning model structure between the 22q11.2DS and control groups. PEB provides a hierarchical Bayesian framework, analogous to a General Linear Model, allowing for robust estimation of group effects on the DCM parameters.

A key advantage of PEB over classical statistical approaches, such as applying independent t-tests to each parameter, lies in its principled handling of estimation uncertainty. DCM parameter estimates are inherently associated with a degree of precision (or uncertainty). PEB explicitly incorporates this uncertainty by weighting the contribution of each subject's parameter estimate to the group-level inference by its posterior precision (inverse variance). Parameters estimated with lower confidence (higher variance) appropriately exert less influence on the group results, whereas classical tests typically ignore this crucial information. This makes PEB particularly robust for analysing complex biophysical models like DCM, where parameters may be estimated with varying degrees of confidence (Friston, Litvak, et al. 2016).

To further enhance robustness and identify the most parsimonious explanation for group differences, the PEB analysis pipeline incorporates automatic Bayesian Model Reduction (BMR) and Averaging (BMA; `spm_dcm_peb_bmc`) (Friston, Litvak, et al. 2016; Penny et al. 2010). BMR systematically compares nested models where specific parameters (or combinations) representing group differences are iteratively 'switched off'. It evaluates the evidence for each reduced model, effectively pruning away parameters that do not contribute meaningfully to explaining between-subject or between-group variability. Subsequently, Bayesian Model Averaging computes weighted averages of the parameter estimates (representing group differences or covariate effects) across the reduced models, where the weighting is determined by the posterior probability (evidence) of each model. This averaging process ensures that the final parameter estimates and inferences are not conditional on a single 'best' model but reflect a consensus across the most plausible explanations supported by the data. Parameters consistently contributing across probable models receive higher weighting, while those unique to less likely models are effectively down-weighted or eliminated.

Finally, inferences within this Bayesian framework are based on the relative evidence supporting the presence versus absence of an effect (e.g., a group difference on a specific connection strength). This is quantified by the posterior probability of the parameter being non-zero. We considered parameters with posterior probabilities exceeding 0.99 as exhibiting strong evidence for an effect.

7.4.1 PEB results

PEB analysis revealed a progressive expansion of synaptic alterations from wake to REM sleep. During wakefulness (supplementary figure 4A), alterations were relatively confined, with the most pronounced difference being decreased NMDA-R-mediated superficial pyramidal self-connections in 22q11.2DS (M = 1.66, SD = 0.99) compared to siblings (M = 2.72, SD = 1.67). AMPA-, GABA-A-, and GABA-B-R-mediated changes were minor during this stage. In N1 (supplementary figure 4B), a stage-dependent reversal was observed, with NMD-RA sp-sp connectivity increased in 22q11.2DS (M = 1.78, SD = 1.18) relative to siblings (M = 1.42, SD = 0.55). N2 sleep (supplementary figure 4C) was marked by a reduction in GABA-A-R-mediated self-inhibition, including si-si (22q11.2DS: M = 1.29, SD = 0.89; siblings: M = 1.52, SD = 0.49), and a tendency toward increased GABA-B-R-mediated inhibition. N3 sleep (supplementary figure 4D) showed a consistent increase in GABA-B-R-mediated inhibition (e.g., dp-dp: M = 1.06, SD = 0.09 vs. M = 0.98, SD = 0.07), while NMDA-R sp-sp connectivity remained lower in 22q11.2DS (M = 1.71, SD = 1.49) than siblings (M = 1.99, SD = 2.22), as in wakefulness. GABA-A and AMPA-R changes were present but less consistent. REM sleep (supplementary figure 4E) exhibited the most extensive alterations. NMDA-R sp-sp connectivity was reduced in 22q11.2DS compared to siblings in REM (M = 2.46, SD = 2.08 vs. M = 2.86, SD = 2.06), consistent with the pattern seen in wake and N3. Exact values for each significant parameter are provided in supplementary table 4.

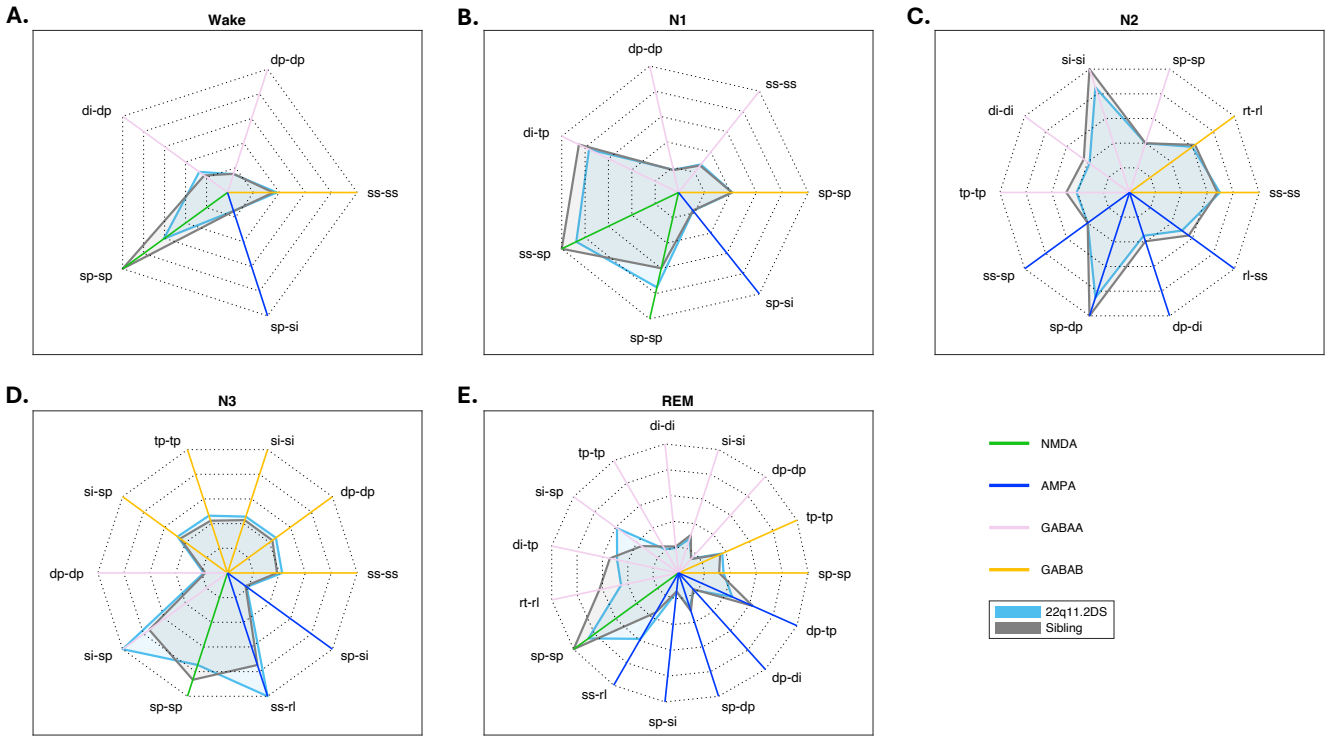

Supplementary figure 4: Receptor-specific alterations across sleep-wake states in 22q11.2DS. Each subplot shows the group mean values for parameters with significant group differences (22q11.2DS (blue) vs. sibling controls (grey)) in a given arousal state, as identified by PEB analysis. Each axis radiating from the centre corresponds to a significant parameter, with abbreviations denoting the neuronal populations involved. The colour of each axis indicates the receptor type mediating the connection: NMDA (green), AMPA (blue), GABA-A (pink), and GABA-B (yellow). Only parameters with significant group differences (posterior probability > 0.99) were displayed for each stage.

Sleep Stage	Parameter	22q11.2DS Mean	22q11.2DS SD	Sibling Mean	Sibling SD
Wake	GABA-B ss-ss	1.036	0.317	0.957	0.133
Wake	GABA-A dp-dp	0.406	0.098	0.413	0.060
Wake	GABA-A di-dp	0.735	0.435	0.607	0.194
Wake	NMDA sp-sp	1.655	0.989	2.722	1.674
Wake	AMPA sp-si	0.406	0.098	0.413	0.060
N1	GABA-B sp-sp	0.984	0.136	0.977	0.127
N1	GABA-A ss-ss	0.655	0.323	0.630	0.400
N1	GABA-A dp-dp	0.426	0.055	0.420	0.043
N1	GABA-A di-tp	1.814	0.598	2.019	0.571
N1	NMDA ss-sp	2.073	1.110	2.368	1.658
N1	NMDA sp-sp	1.776	1.180	1.418	0.548
N1	AMPA sp-si	0.426	0.055	0.420	0.043
N2	GABA-B ss-ss	1.058	0.192	1.028	0.174
N2	GABA-B rt-rl	0.909	0.088	0.947	0.112
N2	GABA-A sp-sp	0.605	0.375	0.606	0.311
N2	GABA-A si-si	1.293	0.889	1.517	0.487
N2	GABA-A di-di	0.579	0.114	0.662	0.167
N2	GABA-A tp-tp	0.620	0.187	0.740	0.295
N2	AMPA ss-sp	0.605	0.375	0.606	0.311
N2	AMPA sp-dp	1.293	0.889	1.517	0.487
N2	AMPA dp-di	0.532	0.206	0.600	0.278
N2	AMPA rl-ss	0.758	0.260	0.855	0.350
N3	GABA-B ss-ss	0.968	0.200	0.878	0.123
N3	GABA-B dp-dp	1.060	0.088	0.983	0.071
N3	GABA-B si-si	1.050	0.078	0.984	0.048
N3	GABA-B tp-tp	1.068	0.133	0.973	0.087
N3	GABA-B si-sp	1.095	0.296	1.036	0.063
N3	GABA-A dp-dp	0.422	0.071	0.395	0.097
N3	GABA-A si-sp	2.298	0.830	1.715	0.868
N3	NMDA sp-sp	1.714	1.486	1.991	2.223
N3	AMPA ss-rl	2.298	0.830	1.715	0.868
N3	AMPA sp-si	0.422	0.071	0.395	0.097
REM	GABA-B sp-sp	0.993	0.137	0.897	0.109
REM	GABA-B tp-tp	1.058	0.155	1.005	0.056
REM	GABA-A dp-dp	0.427	0.125	0.412	0.096
REM	GABA-A si-si	0.793	0.370	0.882	0.345
REM	GABA-A di-di	0.552	0.155	0.588	0.083
REM	GABA-A tp-tp	0.607	0.239	0.675	0.230
REM	GABA-A si-sp	1.680	0.758	1.008	0.493
REM	GABA-A di-tp	1.387	0.601	1.550	0.482
REM	GABA-A rt-rl	1.297	0.888	1.789	1.079
REM	NMDA sp-sp	2.459	2.078	2.863	2.061
REM	AMPA ss-rl	1.680	0.758	1.008	0.493
REM	AMPA sp-si	0.427	0.125	0.412	0.096
REM	AMPA sp-dp	0.793	0.370	0.882	0.345
REM	AMPA dp-di	0.508	0.237	0.481	0.120
REM	AMPA dp-tp	1.297	0.888	1.789	1.079

Supplementary table 4: Group means and standard deviations for each significant parameter and sleep stage.

7.5 Individual parameter perturbations

To identify the most effective synaptic adjustments for aligning 22q11.2DS neural activity with control patterns, we systematically perturbed individual synaptic parameters and measured their effects on power spectral alignment. For each sleep stage, we analysed the effect sizes and significance of adjustments across different receptor systems and cell-type connections (supplementary figure 5).

Notably, NMDA-R sp-sp and NMDA-R sp-ss connections were most consistently among the top parameter adjustments across sleep stages. This finding was robust across both individual connection perturbations and global receptor-wide adjustments (main body section 3.3).

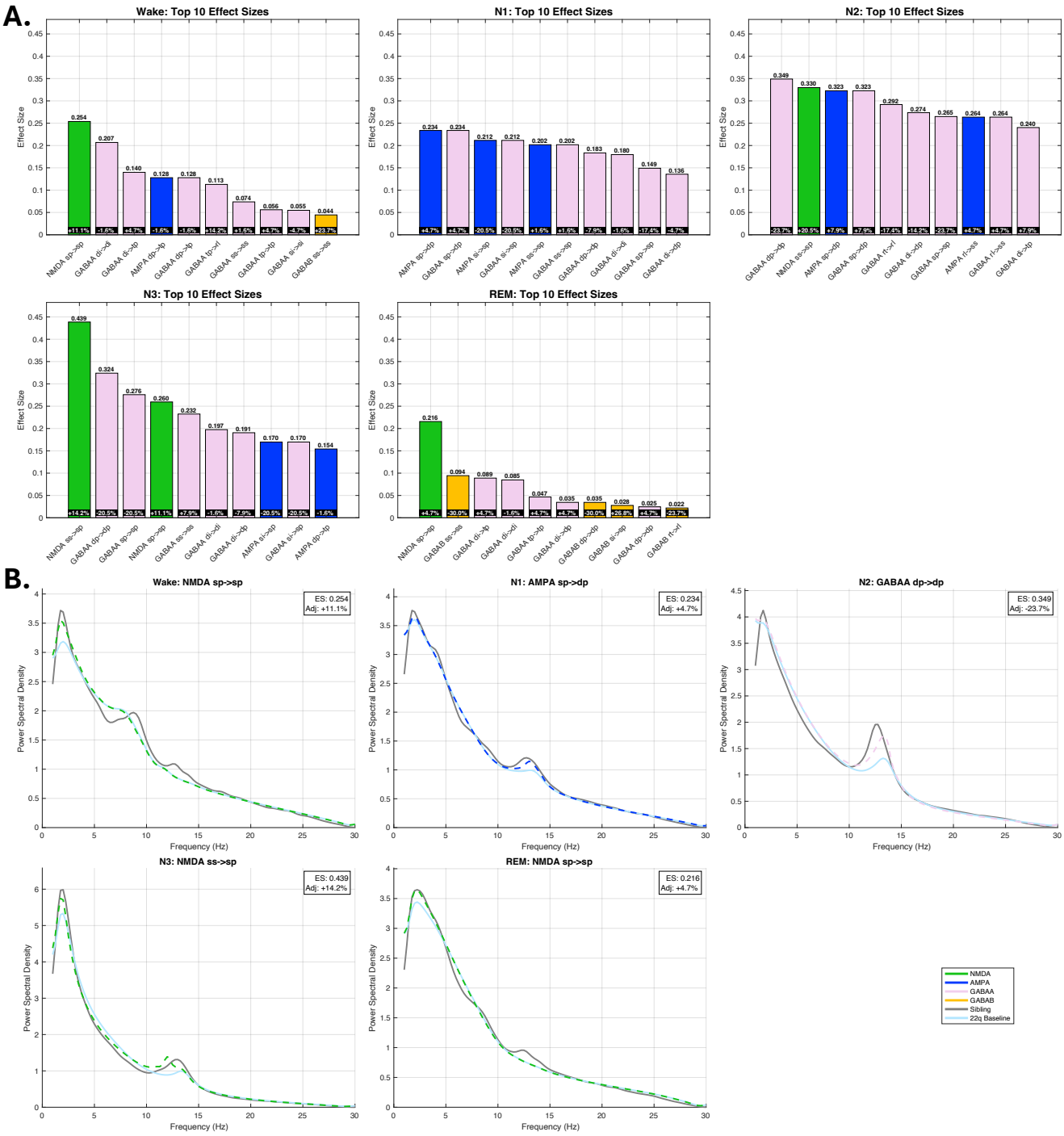

Supplementary figure 5: Impact of Receptor-Specific Perturbations on EEG Spectral Power. A. (Bar Plots): Each panel represents the single best adjustment (in % with positive values indicating necessary increase and negative values decrease in synaptic gain) for the top 10 receptor-connection pairs that produced a significant improvement in aligning the 22q11.2DS model's PSD with the sibling control data. For each pair, the optimal adjustment percentage (in the inserted black boxes) and the corresponding maximum effect size are shown. **B. (Power Spectral Density Plots):** Each panel in the bottom row shows the Power Spectral Density (y-axis) across frequencies (x-axis, 0-30 Hz). The light blue line represents the "22q11.2DS Baseline" spectrum. The grey line represents the sibling PSD. The coloured dashed line indicates the receptor type of the perturbation that achieved the overall "best alignment" for that sleep stage. The Effect Size (ES) and Adjustment percentage (Adj) displayed in each PSD plot quantify the effectiveness of this best perturbation in shifting the 22q11.2DS spectrum towards the sibling spectrum.

7.6 Regression Model Selection for Paramater-Psychiatric/Cognitive Symptom Relationships

Our analysis followed a two-step approach: first using LASSO regression for feature selection, followed by appropriate regression models for the selected features based on their distribution characteristics.

7.6.1 Feature Selection

To manage the high dimensionality of our predictor space relative to our sample size, we first employed LASSO regression (Tibshirani 1996) with 5-fold cross-validation to determine the optimal penalty parameter (λ). This approach helped identify the most relevant synaptic parameters while reducing the risk of overfitting. We acknowledge that even with LASSO regularisation, the relatively small sample size compared to the number of predictors remains a limitation of our analysis, suggesting our results should be interpreted as exploratory and requiring validation in larger cohorts.

7.6.2 Regression Models for Selected Features

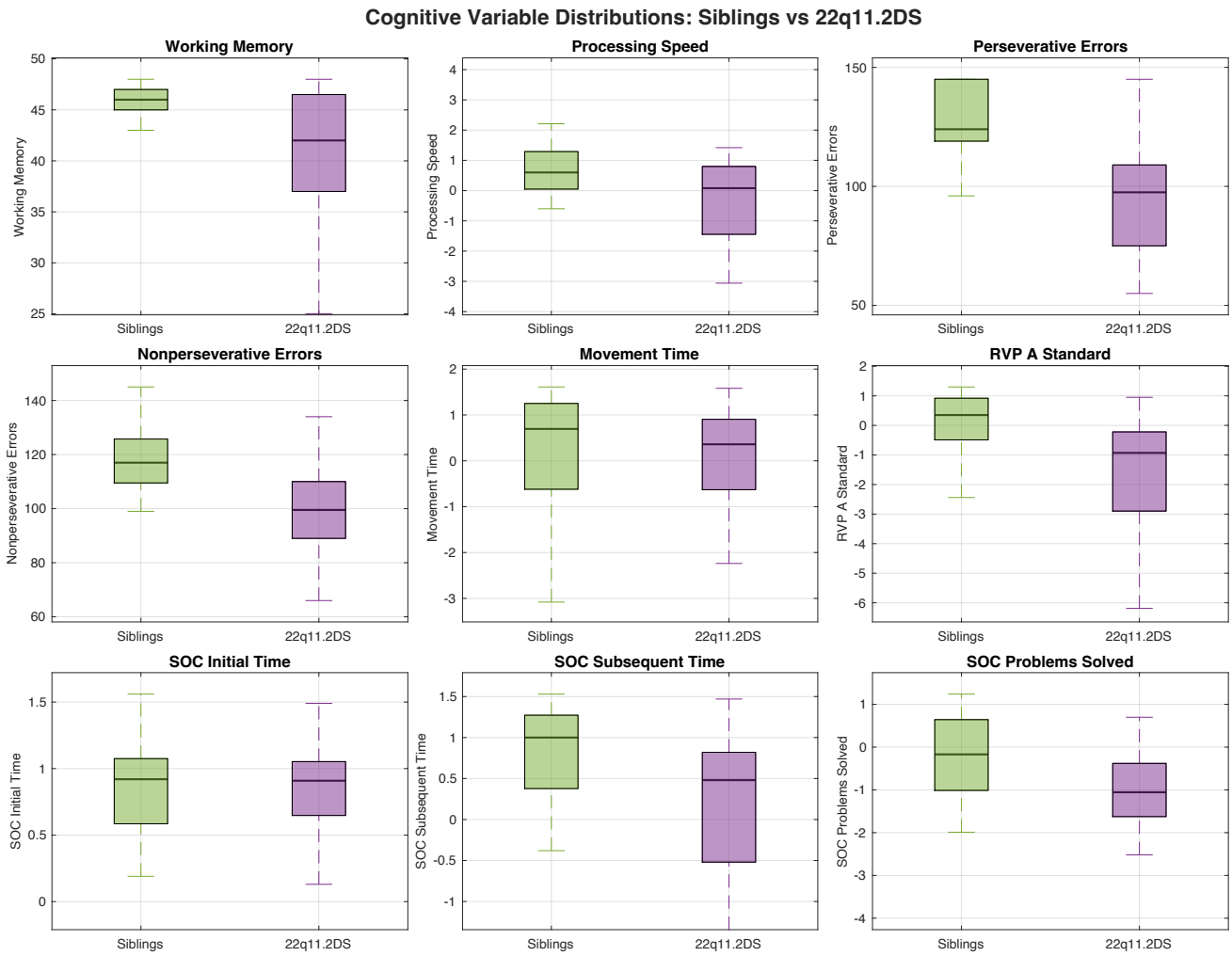

Supplementary figure 6: Cognitive Variable Distributions in 22q11.2DS and Siblings. Box plots showing the distribution of cognitive measures between 22q11.2DS carriers (purple) and sibling controls (green). Measures include working memory performance, processing speed, perseverative and nonperseverative errors (executive function), movement time, sustained attention (RVP A' Standard), and planning ability (SOC Initial Time, Subsequent Time, and Problems Solved). The boxes show the interquartile range with the median line, whiskers extend to 1.5 times the interquartile range.

Following LASSO feature selection, we analysed the relationships between selected features and outcome measures using appropriate regression models based on their distribution characteristics:

For psychiatric measures, count data (ADHD, anxiety, ASD symptoms, and sleep disturbances) were first tested for overdispersion. When the variance significantly exceeded the mean ($p < 0.05$), indicating overdispersion, we used negative binomial regression instead of Poisson regression. For all our count measures, overdispersion was present, leading to the use of negative binomial models. Psychotic experiences were analysed using logistic regression as this was a binary outcome measure.

For cognitive measures, Working Memory and SOC Problems Solved were analysed using linear regression after confirming normality using Shapiro-Wilk tests (Royston 1992) ($p > 0.05$) and Q-Q plots. Processing Speed and SOC Initial/Subsequent Time measures required log transformation, before linear regression analysis. RVP A', being bounded between 0 and 1 and showing no significant deviation from normality (Shapiro-Wilk test, $p > 0.05$), was analysed using linear regression. Perseverative and Nonperseverative Errors showed significant overdispersion in initial Poisson models and were therefore analysed using negative binomial regression (supplementary figure 6).